
TRAINING A FOUNDATION MODEL TO REPRESENT GRAPHS AS VECTORS

A PREPRINT

Qi Feng

School of Data Science

The Chinese University of Hong Kong, Shenzhen
Shenzhen, China
qifeng@link.cuhk.edu.cn

Jicong Fan

School of Data Science

The Chinese University of Hong Kong, Shenzhen
Shenzhen, China
fanjicong@cuhk.edu.cn

February 5, 2026

ABSTRACT

This paper aims to train a graph foundation model that is able to represent any graph as a vector preserving structural and semantic information useful for downstream graph-level tasks such as graph classification and graph clustering. To learn the features of graphs from diverse domains while maintaining strong generalization ability to new domains, we propose a multi-graph-based feature alignment method, which constructs weighted graphs using the attributes of all nodes in each dataset and then generates consistent node embeddings. To enhance the consistency of the features from different datasets, we propose a density maximization mean alignment algorithm with guaranteed convergence. The original graphs and generated node embeddings are fed into a graph neural network to achieve discriminative graph representations in contrastive learning. More importantly, to enhance the information preservation from node-level representations to the graph-level representation, we construct a multi-layer reference distribution module without using any pooling operation. We also provide a theoretical generalization bound to support the effectiveness of the proposed model. The experimental results of few-shot graph classification and graph clustering show that our model outperforms strong baselines.

Keywords Graph Neural Networks · Graph Foundation Model · Graph Representation

1 Introduction

Graph data is a fundamental and widely prevalent form of structured data, representing entities as nodes and their relationships as edges. It plays a crucial role in diverse domains, including social networks, biological systems, citation networks, recommendation systems, and knowledge graphs. Given its ability to model complex relational patterns, graph data analysis has become a key focus in machine learning and data mining. In node-level tasks, the training set is usually a single but large graph, on which each node represents a sample. Node-level tasks include node embedding or representation [Grover and Leskovec, 2016, Cai et al., 2018], node classification [Kipf and Welling, 2017], node clustering [Wang et al., 2023], link prediction [Martínez et al., 2016], etc. For example, node classification might involve categorizing users in a social network, while link prediction could be used to recommend new connections.

On the other hand, graph-level tasks operate on entire graphs, where a dataset is composed of numerous graphs, and each graph is treated as a sample. Graph-level tasks address broader challenges such as graph comparison [Kobler et al., 2012], representation learning [Sun et al., 2020], classification [Xu et al., 2019], clustering [Cai et al., 2024], generation [Liao et al., 2019], etc. Graph comparison often relies on graph kernels [Gärtner et al., 2003, Vishwanathan et al., 2010, Shervashidze et al., 2011] or distances [Bunke, 1997, Zeng et al., 2009, Mémoli, 2011, Bento and Ioannidis, 2018] or deep learning methods [Sun and Fan, 2024] to measure similarity between different graphs, while graph representation learning aims to encode entire graphs into compact, informative embeddings for downstream tasks [You et al., 2020, 2021, Sun et al., 2023a]. Graph classification, for example, is critical in chemistry for predicting molecular properties

[Gilmer et al., 2017, Wang and Fan, 2024], whereas graph generation enables the creation of novel structures, such as drug-like molecules in computational biology [Hoogeboom et al., 2022].

The aforementioned methods of node-level learning and graph-level learning are dataset-specific. That means, for one dataset, we have to train a new model, e.g., a graph neural network, to solve the corresponding problem. This leads to the following two limitations. First, training a model from scratch is very time-consuming, and it requires model selection and parameter tuning, which brings inconvenience to practical applications. Second, knowledge from historical data or tasks in the same domain or similar domains cannot be exploited well. To address the limitations, recently, graph foundation models (GFM) have become an increasingly prominent area of research in graph data analysis due to their ability to harness diverse datasets to enhance performance across multiple tasks and domains. Emerging studies [Galkin et al., 2023, Zheng et al., 2023] indicate that GFM exhibit strong generalization capabilities, even when applied to previously unseen graph structures. Mao et al. [2024] categorizes GFM into three distinct types according to their adaptability: domain-specific, task-specific, and primitive models. Domain-specific GFM [Xia et al., 2023, Zhang et al., 2023, Zheng et al., 2023] focus on extracting universal features within a specialized domain, enabling a single model to address multiple related tasks while often surpassing the performance of dedicated task-specific models. Task-specific GFM [Galkin et al., 2024, Zhao et al., 2024a, Lachi et al., 2024], on the other hand, are trained on extensive datasets to excel at particular tasks, making them particularly valuable in domains where data is scarce. Primitive GFM [Tang et al., 2024a] offer greater flexibility, but are limited in applicability to specific datasets and tasks.

One key challenge in building GFM is that graph patterns from different domains exhibit significant variation [Galkin et al., 2023], which is evident in both structural and feature representations. For example, in molecular graphs [Yang et al., 2016], the structure encodes 3D spatial arrangements and atomic bonds, while node features represent chemical properties. Conversely, in social networks [Dwivedi et al., 2023], the structure reflects user connections, and node features correspond to user profiles. These distribution differences make it difficult for a single model to learn domain-agnostic representations. A promising approach involves transforming both graph structures and node features into textual formats, then employing large language models (LLMs) to derive unified representations [Fatemi et al., 2023, Liu et al., 2023a, Tang et al., 2024b, Wang et al., 2024a]. Another approach is to improve existing graph learning paradigms [Liu et al., 2025] through innovations in the aspects of the backbone [Rong et al., 2020], pre-training [Qiu et al., 2020, You et al., 2020, Yu et al., 2025a], and adaptations [Fu et al., 2025, Yu et al., 2025b, Wang et al., 2025a]. More work on GFM can be found in Appendix B.

Despite these excellent works on GFM, there are still a few limitations and much room for improvement. First, in LLM-based GFM, converting graph data into text may lose important information of topological structures and node features of graphs [Yu et al., 2025a], and the computation cost is often high due to the large sizes of LLMs. Second, most of the existing GFM were proposed for node-level tasks [Zhao et al., 2024a, Wei et al., 2024, Wang et al., 2025a] rather than graph-level tasks [Yu et al., 2025b, Fu et al., 2025]. Lastly, training a single graph model across diverse domains while maintaining strong generalization ability to new domains or various downstream tasks remains challenging.

This work proposes a GFM for graph-level tasks across diverse domains. Our contributions are:

- We present a novel multi-graph construction based feature alignment strategy, which enables our GFM to exploit the association of samples without influenced by the semantic changes across datasets or domains.
- We provide a novel density-maximization algorithm to enhance the alignment of cross-domain features and prove its convergence theoretically. It is also useful in handling graphs without inherent node attributes.
- We develop a multi-layer reference distribution module to improve the graph-level representation since simply performing pooling will result in significant information loss of node embeddings.
- We provide a generalization error bound to support the effectiveness of our model theoretically.

The experiments in the tasks of few graph classification and graph-level clustering demonstrate the effectiveness and superiority of our model in comparison to state-of-the-art competitors.

2 Related Work

Language Model-Free GFM Many studies have explored training GFM using the “pre-train and adaptation” paradigm, leveraging message-passing or transformer-based GNN backbones. These approaches typically employ contrastive or generative self-supervised learning for pretraining, followed by fine-tuning a subset of model parameters to adapt to downstream tasks or datasets [Liu et al., 2025]. Contrastive methods including GCC [Qiu et al., 2020], InfoGraph [Sun et al., 2019], DGI [Veličković et al., 2019], SimGRACE [Xia et al., 2022], GCOPE [Zhao et al., 2024b] maximize agreement between augmented views to learn transferable representations, while generative methods

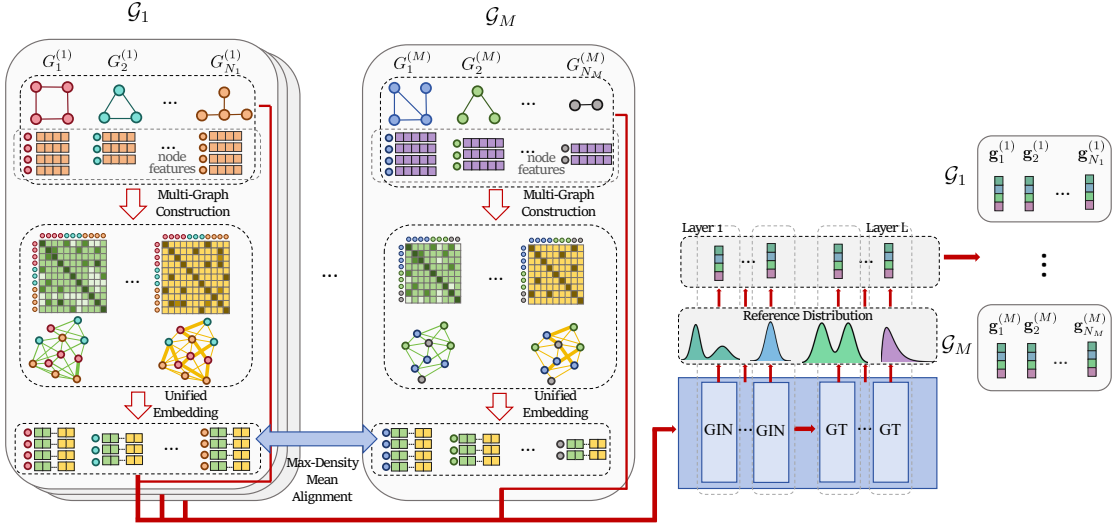


Figure 1: Flow-chart of the proposed method GraphVec-FM. $\mathcal{G}_1, \dots, \mathcal{G}_M$ are M datasets from different domains. The model represents each graph $G_i^{(j)}$ as a single vector $\mathbf{g}_i^{(j)}$ that can be used in graph-level downstream tasks.

[Hou et al., 2022, 2023] pre-train via graph reconstruction or property prediction. Recently, graph prompt tuning [Sun et al., 2022, Fang et al., 2023, Sun et al., 2023b, Liu et al., 2023b, Fu et al., 2025] has emerged to bridge the pretraining–downstream gap, and many recent GFMs adopt this paradigm [Yuan et al., 2025a, Yu et al., 2025c]. However, these works mainly emphasize adaptation, leaving the problem of learning unified graph representations underexplored. Due to space limitations, we defer more discussion of **Language Model-Free GFMs** and the related work on **LLM-based GFMs** and **GFM for Graph-Level Tasks** to Appendix B.

3 Problem Formulation

First of all, the major notations used in this paper are shown in Table 5. Let $\mathcal{D} = \{\mathcal{G}_1, \mathcal{G}_2, \dots, \mathcal{G}_M\}$ be a union of M datasets of labeled graphs from M different domains, where $\mathcal{G}_j = \{(G_1^{(j)}, y_1^{(j)}), (G_2^{(j)}, y_2^{(j)}), \dots, (G_{N_j}^{(j)}, y_{N_j}^{(j)})\}$. Here, each graph $G_i^{(j)}$ is denoted as $G_i^{(j)} = (\mathbf{A}_i^{(j)}, \mathbf{X}_i^{(j)}, y_i^{(j)})$, where $\mathbf{A}_i^{(j)} \in \mathbb{R}^{n_i^{(j)} \times n_i^{(j)}}$ denotes the adjacency matrix, $\mathbf{X}_i^{(j)} \in \mathbb{R}^{n_i^{(j)} \times d^{(j)}}$ denotes the node attribute matrix, $n_i^{(j)}$ denotes the number of nodes, $d^{(j)}$ denotes the number of attributes, and $y_i^{(j)}$ denotes the graph label. Our goal is to use \mathcal{D} to train a GFM, denoted as

$$F : \mathbb{G} \rightarrow \mathbb{R}^r \quad (1)$$

to represent any graph from the space \mathbb{G} as an r -dimensional vector that is useful in downstream tasks such as graph classification, where \mathbb{G} denotes the set of all graphs in the form of (\mathbf{A}, \mathbf{X}) . Therefore, F serves as a universal graph representation model.

To learn F from \mathcal{D} , we need to address these challenges:

- **Attributes inconsistency** The node attributes of graphs from different domains are different and not comparable at all. Thus the node attributes in \mathcal{D} cannot be fed into F directly.
- **Attributes absence** Many graph datasets do not contain node attributes, making them very different from graph datasets with node attributes. The heuristic method of constructing node attributes, such as using node degrees, does not comply with the semantic attributes of other datasets.
- **Information loss in pooling** Although there have been a few advanced graph pooling methods [Liu et al., 2022], converting nodes' embeddings into a single vector cannot fully utilize the information.

4 Methodology

4.1 Multi-Graph based Feature Alignment

As mentioned, the node features of different domain graph datasets may vary significantly in semantics and dimensions. To capture domain-invariant features, we focus on the relationships among nodes across the entire dataset rather than the original features. The reason is that in many machine learning problems, using the relationships between samples or a graph constructed from the dataset can provide effective solutions. For instance, in spectral clustering [Ng et al., 2001], we use a similarity graph rather than the original features; in kernel support vector machine [Cortes and Vapnik, 1995], we can use a Gaussian kernel matrix, which is a similarity matrix of the data points. **Global Graph Construction** For each graph dataset \mathcal{G}_j , $j \in [M]$, we propose to construct a similarity graph over all nodes in the dataset using a Gaussian kernel function, i.e.,

$$\mathbf{K}_\lambda^{(j)} = \left[\exp \left(-\frac{\|\mathbf{x}_u - \mathbf{x}_v\|_2^2}{2\lambda\mu^2} \right) \right]_{u,v=1}^{\bar{N}_j}, \quad \bar{N}_j = \sum_{i=1}^{N_j} n_i^{(j)} \quad (2)$$

where \mathbf{x}_i is the i -th row of $\mathbf{X} := \left[\mathbf{x}_i^{(j)} \right]_{i=1}^{N_j}$ (vertical concatenation), μ is the mean of the pairwise distances between all nodes in the dataset, and λ controls the bandwidth of the kernel. This setting ensures *translation, rotation, and scaling invariance*, which is important to extract comparable features across diverse datasets. $\mathbf{K}_\lambda^{(j)}$ is the adjacency matrix of this global graph of the nodes in \mathcal{G}_j . Note that a single $\mathbf{K}_\lambda^{(j)}$ exploits partial information of the node attributes of \mathcal{G}_j and the optimal setting of λ remains an open problem. Therefore, we use a number of different values for λ , e.g. $\lambda_1, \lambda_2, \dots, \lambda_Q$, to construct **multiple global graphs** for the nodes in \mathcal{G}_j :

$$\mathcal{K}^{(j)} := \left\{ \mathbf{K}_{\lambda_1}^{(j)}, \mathbf{K}_{\lambda_2}^{(j)}, \dots, \mathbf{K}_{\lambda_Q}^{(j)} \right\}, \quad j \in [M] \quad (3)$$

Note that the diversity of $\mathcal{K}^{(j)}$ can be further enhanced if more kernel families, e.g., $k(\mathbf{x}_u, \mathbf{x}_v) = \exp(-\alpha\|\mathbf{x}_u - \mathbf{x}_v\|_1)$, are considered.

Consistent Embeddings from Global Graphs For $\mathbf{K}_{\lambda_q}^{(j)}$, we compute \bar{d} -dimensional node embeddings using singular value decomposition (SVD):

$$\mathbf{Z}_{\lambda_q}^{(j)} = \mathbf{U}_{\bar{d}} \mathbf{\Sigma}_{\bar{d}}^{1/2}, \quad \mathbf{K}_{\lambda_q}^{(j)} = \mathbf{U} \mathbf{\Sigma} \mathbf{V}^\top \quad (4)$$

where $\mathbf{U}_{\bar{d}} \in \mathbb{R}^{\bar{N}_j \times \bar{d}}$ is composed of the first \bar{d} columns of \mathbf{U} and $\mathbf{\Sigma}_{\bar{d}}$ is a diagonal matrix consisting of the first (largest) \bar{d} singular values. Then the final node feature matrix is obtained by concatenating embeddings from all scales, i.e.,

$$\mathbf{Z}^{(j)} = \left[\mathbf{Z}_{\lambda_1}^{(j)}, \dots, \mathbf{Z}_{\lambda_Q}^{(j)} \right] = \begin{bmatrix} \mathbf{Z}_1^{(j)} \\ \vdots \\ \mathbf{Z}_{\bar{N}_j}^{(j)} \end{bmatrix} \in \mathbb{R}^{\sum_{i=1}^{N_j} n_i^{(j)} \times Q\bar{d}}, \quad (5)$$

where $j \in [M]$. For datasets without node attributes, we generate node attributes using the truncated SVD of the self-looped adjacency matrix, i.e.,

$$\mathbf{X}_i^{(j)} = \text{SVD} \left(\mathbf{A}_i^{(j)} + \mathbf{I}_{n_i^{(j)}} \right) \in \mathbb{R}^{n_i \times \bar{d}} \quad (6)$$

where $\text{SVD}(\cdot)$ returns the singular vectors corresponding to the top- \bar{d} singular values, similar to (4). Then we apply (2), (3), (4), and (5) to $\mathbf{X}_i^{(j)}$ to generate unified node embeddings. For large datasets, the Nyström approximation [Williams and Seeger, 2000] can be employed to accelerate the computation of the kernel matrix and SVD.

4.2 Density Maximization based Mean Alignment

In SVD, individual singular vectors have arbitrary signs [Bro et al., 2008]. This sign ambiguity may make the embeddings of two similar graphs very different, leading to significant difficulties in both the training and testing stages. Moreover, if two singular values are the same, the order of the corresponding singular vectors cannot be determined, which further increase the difficulty in learning. In machine learning, to ensure learnability and generalization, we require that the training samples and the testing samples are from the same distribution, or at least, their means are similar. Therefore, we proposed to align the mean embeddings of different graphs via maximizing the density.

Specifically, consider the SVD embeddings of $M \times Q$ graphs generated by the method in Section 4.1, for each λ_q , we compute the mean vectors of the embedding matrices $\mathbf{Z}_{\lambda_q}^{(j)}$ as $\boldsymbol{\mu}_j = \frac{1}{\bar{N}_j} \mathbf{Z}_j^\top \mathbf{1}_{\bar{N}_j}$, where $j \in [M]$ and we have dropped the subscript λ_q to simplify the notation for the following operations. For each graph j , we introduce an orthonormal matrix

Algorithm 1 Max-Density Mean Alignment**Input:** $\mu_1, \mu_2, \dots, \mu_M; \gamma > 0; \eta > 0; T$.

- 1: Initialization: $\mathbf{R}_j^{(0)} = \mathbf{I}_{\bar{d}}, \forall j \in [M]$
- 2: $w_{ij} = \exp(-\gamma(\|\mu_i\|^2 + \|\mu_j\|^2)), (i, j) \in [M] \times [M]$
- 3: **for** $t = 1$ to T **do**
- 4: $k_{ij}^{(t-1)} = \exp(2\gamma \langle \mathbf{R}_i^{(t-1)} \mu_i, \mathbf{R}_j^{(t-1)} \mu_j \rangle), (i, j) \in [M] \times [M]$
- 5: **for** $i = 1$ to M **do**
- 6: $\mathbf{H}_i^{(t)} = \sum_j w_{ij} k_{ij}^{(t-1)} \mathbf{R}_j^{(t-1)} \mu_j \mu_i^\top + \eta \mathbf{R}_i^{(t-1)}$
- 7: SVD: $\mathbf{H}_i^{(t)} = \mathbf{U}_i \mathbf{S}_i \mathbf{V}_i^\top$
- 8: $\mathbf{R}_i^{(t)} = \mathbf{U}_i \mathbf{V}_i^\top$
- 9: **end for**
- 10: **end for**

Output: $\mathbf{R}_1, \mathbf{R}_2, \dots, \mathbf{R}_M$ **Algorithm 2** Pre-training model**Input:** Train datasets: $\mathcal{D} = \{\mathcal{G}_j\}_{j=1}^M$

- 1: Compute $\{\mathbf{Z}^{(j)}\}_{j=1}^M$ using (4) and (5)
- 2: $\{\mathbf{R}_j^{\lambda_q}\}_{j=1}^M \leftarrow$ Algorithm 1
- 3: $\mathbf{Z}_{\lambda_q}^{(j)} \leftarrow \mathbf{Z}_{\lambda_q}^{(j)} \mathbf{R}_j^{(\lambda_q)^\top}, q \in [Q], j \in [M]$
- 4: **repeat**
- 5: **for** $j = 1$ to M **do**
- 6: **for** $i = 1$ to S **do**
- 7: Sample $\{\mathbf{G}_i^{(j)} = (\mathbf{Z}_i^{(j)}, \mathbf{A}_i^{(j)})\}_{i \in \mathcal{B}}$
- 8: $\mathbf{g}_i^{(j)} \leftarrow F_{\mathcal{W}, \mathcal{V}, \gamma}(\mathbf{A}_i^{(j)}, \mathbf{Z}_i^{(j)}), i \in \mathcal{B}$
- 9: $\mathcal{W} \leftarrow \mathcal{W} + \alpha_1 \nabla_{\mathcal{W}} \mathcal{L}(\mathcal{W}, \mathcal{V}, \gamma)$
 $\mathcal{V} \leftarrow \mathcal{V} + \alpha_1 \nabla_{\mathcal{V}} \mathcal{L}(\mathcal{W}, \mathcal{V}, \gamma)$
 $\gamma \leftarrow \gamma + \alpha_2 \nabla_{\gamma} \mathcal{L}(\mathcal{W}, \mathcal{V}, \gamma)$
- 10: **end for**
- 11: **end for**
- 12: **until** Convergence conditions are met

Output: Pretrained model $F_{\mathcal{W}, \mathcal{V}, \gamma}$

$\mathbf{R}_j \in \mathbb{R}^{\bar{d} \times \bar{d}}$, which will transform μ_j as $\mathbf{R}_j \mu_j, j \in [M]$, which means $\mathbf{R}_j \mathbf{Z}_{\lambda_q}^{(j)}$ is equivalent to $\mathbf{Z}_{\lambda_q}^{(j)}$ in preserving the information of $\mathbf{K}_{\lambda_q}^{(i)}$. We align all mean vectors using the corresponding orthonormal matrices by maximizing the density of the mean vectors. The density of each mean vector can be calculated by the kernel density estimation [Parzen, 1962]:

$$\hat{p}(\mu) = \frac{1}{M} \sum_{j=1}^M \frac{1}{(2\pi h)^{\bar{d}/2}} \exp\left(-\frac{\|\mu - \mu_j\|^2}{2h}\right) \quad (7)$$

where we use the Gaussian kernel with hyperparameter h . Let \mathcal{R} be the set of all orthonormal matrices of size $\bar{d} \times \bar{d}$, i.e., $\mathcal{R} = \{\mathbf{R} \in \mathbb{R}^{\bar{d} \times \bar{d}} : \mathbf{R}^\top \mathbf{R} = \mathbf{I}_{\bar{d}}\}$. Then we maximize the total density of the M mean vectors:

$$\underset{\mathbf{R}_j \in \mathcal{R}, j \in [M]}{\text{maximize}} \frac{1}{N} \sum_{i=1}^M \sum_{j=1}^M \frac{1}{(2\pi h)^{\bar{d}/2}} \exp\left(-\frac{\|\mathbf{R}_i \mu_i - \mathbf{R}_j \mu_j\|^2}{2h}\right) \quad (8)$$

Letting $\gamma = \frac{1}{2h}$, (8) is equivalent to the following problem

$$\begin{aligned} & \underset{\mathbf{R}_j \in \mathcal{R}, j \in [M]}{\text{maximize}} \frac{1}{M} \sum_{i=1}^M \sum_{j=1}^M \exp(-\gamma \|\mathbf{R}_i \mu_i - \mathbf{R}_j \mu_j\|^2) \\ & \triangleq \mathcal{L}(\{\mathbf{R}_j\}_{j=1}^M) \end{aligned} \quad (9)$$

The optimization is non-trivial due to the orthonormal constraints and the exponential functions. We propose an efficient algorithm in Algorithm 1. The detailed derivation for the algorithm is introduced in Appendix C. Theorem 4.1 provides a convergence guarantee for the optimization.

Theorem 4.1. Let $\{\mathcal{L}(\{\mathbf{R}_j^{(t)}\}_{j=1}^M)\}_t$ and $\{\{\mathbf{R}_j^{(t)}\}_{j=1}^M\}_t$ be the sequences given by Algorithm 1. Then for any $\eta > 0$, it holds that:

- (a) $\{\mathcal{L}(\{\mathbf{R}_j^{(t)}\}_{j=1}^M)\}_t$ is non-decreasing, i.e., $\mathcal{L}(\{\mathbf{R}_j^{(t)}\}_{j=1}^M) \geq \mathcal{L}(\{\mathbf{R}_j^{(t-1)}\}_{j=1}^M)$;
- (b) $\{\{\mathbf{R}_j^{(t)}\}_{j=1}^M\}_t$ is convergent, i.e., $\mathbf{R}_j^{(t)} - \mathbf{R}_j^{(t-1)} \rightarrow \mathbf{0}$ when $t \rightarrow \infty$.

Once $\mathbf{R}_1, \dots, \mathbf{R}_M$ are optimized, we modify the embeddings of the $M \times Q$ global graphs as

$$\mathbf{Z}_{\lambda_q}^{(j)} \leftarrow \mathbf{Z}_{\lambda_q}^{(j)} \mathbf{R}_j^{(\lambda_q)^\top}, \quad q \in [Q], j \in [M], \quad (10)$$

where $\mathbf{R}_i^{(\lambda_q)}$ denotes the \mathbf{R}_j we obtained for the kernel embeddings given by the q -th kernel function. Recalling (5) and using (10), we here obtain the modified embeddings $\mathbf{Z}_1^{(j)}, \dots, \mathbf{Z}_{N_j}^{(j)}, j \in [M]$. It is worth noting that Algorithm 1 can also be applied to the generated attributes by (6) of graphs without inherent node attributes.

4.3 GIN and Graph Transformer based Model

To design a universal graph representation model F , we incorporate two main components: a GIN module f [Xu et al., 2019] and a graph transformer (GT) [Rampášek et al., 2022] module g . We build GIN encoder on top of transformer

encoder $g_\psi \circ f_\theta(\cdot)$, where θ and ψ are the parameters. The GIN encoder specializes in learning local representations of the structure of a node's immediate neighborhood, while the transformer computes all pairwise node interactions, enabling global reasoning through attention mechanisms. The node representations of $G_i^{(j)}$ obtained from the model can be formulated as

$$\mathbf{H}_i^{(j)} = g_\psi \circ f_\theta \left(\mathbf{A}_i^{(j)}, \mathbf{Z}_i^{(j)} \right) \parallel f_\theta \left(\mathbf{A}_i^{(j)}, \mathbf{Z}_i^{(j)} \right) \quad (11)$$

where $i \in [N_j]$ and $j \in [M]$. For convenience, we let $\mathcal{W} = \{\psi, \theta\}$, which is the set of all parameters of the GIN and GT.

4.4 Reference Distribution based Global Graph Representation

Current GFMs often use a single graph pooling method to obtain the final graph representation, which collects only first-order statistics and therefore leads to a loss of structural or semantic information. To obtain more informative graph embeddings from node embedding matrices, we adapt the reference learning module proposed by [Wang and Fan, 2024] to a deep and stacked version.

Specifically, the reference distribution (RD) module treats the nodes' latent representations of each graph as a discrete distribution and then measures the similarity between the latent graph's distribution and the learnable reference distribution to obtain the graph representation vectors. Hence, it can effectively preserve the information of node embeddings. Suppose for a certain layer $l \in [L]$ in the backbone, we have R reference discrete distributions $\{\mathbf{V}_1^{(l)}, \mathbf{V}_2^{(l)}, \dots, \mathbf{V}_R^{(l)}\} \triangleq \mathcal{V}^{(l)}$, each $\mathbf{V}_b^{(l)} \in \mathbb{R}^{m \times d}$ can be understood as node embeddings of a virtual graph with m nodes, drawn from one of R different distributions with m nodes. To get the graph representations from node embedding matrix $\mathbf{H}_i^{(j,l)}$, we measure the similarity between the graph $G_i^{(j)}$ and the reference distributions $\{\mathbf{V}_b^{(l)}\}_{b=1}^R$. Letting ξ be a similarity measure between two distributions, the similarity between the graph $G_i^{(j)}$ and the reference distribution $\mathbf{V}_b^{(l)}$ is

$$s_i^{(j,l)} = \xi \left(\mathbf{H}_i^{(j,l)}, \mathbf{V}_b^{(l)} \right), \quad b \in [R] \quad (12)$$

We let ξ be the negative kernelized Maximum Mean Discrepancy (MMD) [Gretton et al., 2012] to be the similarity measure ξ and have

$$\begin{aligned} s_{i,b}^{(j,l)} &= -\text{MMD} \left(\mathbf{H}_i^{(j,l)}, \mathbf{V}_b^{(l)} \right) \\ &= -\left\| \frac{1}{n_i} \sum_{p=1}^{n_i} \phi \left(\mathbf{h}_p^{(j,l)} \right) - \frac{1}{m} \sum_{q=1}^m \phi \left(\mathbf{v}_q^{(b,l)} \right) \right\|_2 \\ &= -\left[\frac{1}{n_i^2} \sum_{p,p' \in [n_i]} k \left(\mathbf{h}_p^{(j,l)}, \mathbf{h}_{p'}^{(j,l)} \right) + \frac{1}{m^2} \sum_{q,q' \in [m]} k \left(\mathbf{v}_q^{(b,l)}, \mathbf{v}_{q'}^{(b,l)} \right) \right. \\ &\quad \left. - \frac{2}{m n_i} \sum_{p \in [n_i], q \in [m]} k \left(\mathbf{h}_p^{(j,l)}, \mathbf{v}_q^{(b,l)} \right) \right]^{\frac{1}{2}} \end{aligned} \quad (13)$$

where ϕ is the high-dimensional feature map induced by a kernel function, $\mathbf{h}_p^{(j)}$ is the p -th row of $\mathbf{H}_i^{(j)}$, $\mathbf{v}_q^{(b)}$ is the q -th row of \mathbf{V}_b , and $k(\mathbf{x}, \mathbf{x}') = \exp(-\gamma \|\mathbf{x} - \mathbf{x}'\|^2)$ is the Gaussian kernel with a learnable parameter γ . We apply the RD module after every layer in both the GT and GIN backbones, allowing the final graph embedding to capture hierarchical information from neighbors at different ranges. The final graph embedding $\mathbf{g}_i^{(j)} \in \mathbb{R}^r$ of graph i in dataset j combines the similarity vector $\mathbf{s}_i^{(j)} = \left\|_{l \in [L]} s_i^{(j,l)} \right\|$ from different layers with a readout vector $\mathbf{p}_i^{(j)}$, i.e.,

$$\mathbf{g}_i^{(j)} = \mathbf{s}_i^{(j)} \parallel \mathbf{p}_i^{(j)}, \quad i \in [N_j], j \in [M] \quad (14)$$

where $\mathbf{p}_i^{(j)} = \text{READOUT}(\mathbf{H}_i^{(j)})$ is obtained using a graph-level pooling operation.

4.5 Model Pre-training

Different datasets $\mathcal{G}_1, \mathcal{G}_2, \dots, \mathcal{G}_M$ may contain varying numbers of classes. To unify the training framework across different datasets and avoid changing classifiers during training, we adopt the supervised contrastive loss (SCL) [Oord et al., 2018]. Therefore, we minimize the following loss

$$\mathcal{L}_{\text{SCL}}(\mathcal{W}, \mathcal{V}, \gamma) = -\sum_{j=1}^M \frac{1}{N_j} \sum_{i=1}^{N_j} \frac{1}{|C(i)|} \sum_{u \in C(i)} \log \left(p_{iu}^{(j)} \right) \quad (15)$$

where $p_{iu}^{(j)} = \exp\left(\zeta(\mathbf{g}_i^{(j)}, \mathbf{g}_u^{(j)})\right) / \sum_{v \neq i}^{N_j} \exp\left(\zeta(\mathbf{g}_i^{(j)}, \mathbf{g}_v^{(j)})\right)$, $\mathbf{g}_i^{(j)} = F_{\mathcal{W}, \mathcal{V}, \gamma}(\mathbf{A}_i^{(j)}, \mathbf{Z}_i^{(j)})$, $\zeta(\mathbf{u}, \mathbf{v}) = \frac{\mathbf{u}^\top \mathbf{v}}{\tau \|\mathbf{u}\| \|\mathbf{v}\|}$, $C(i)$ denotes the set of samples from the same class as $\mathbf{g}_i^{(j)}$, and τ is a temperature hyperparameter. This objective encourages graphs from the same class to be close in the embedding space while pushing apart samples from different classes. For convenience, we call our method Graph Vectorization Foundation Model (GraphVec-FM).

A key appeal of foundation models lies in their ability to leverage large-scale unlabeled data. GraphVec-FM can also be adapted to unsupervised pre-training scenario. Let $P(i)$ be the set of positive samples of G_i obtained by augmentation, the unsupervised contrastive loss (USL) can be represented as

$$\mathcal{L}_{\text{UCL}}(\mathcal{W}, \mathcal{V}, \gamma) = - \sum_{j=1}^M \frac{1}{N_j} \sum_{i=1}^{N_j} \frac{1}{|P(i)|} \sum_{u \in P(i)} \log(p_{iu}^{(j)}) \quad (16)$$

4.6 Model Testing

When applying the pretrained model to graph-level downstream tasks, the output embeddings generated by the model can be directly utilized as input features for other machine learning models. Specifically, in few-shot graph classification, the mean alignment algorithm need to be performed on both train graphs and test graphs, the detailed formulation and algorithm are in Appendix G.2.

Table 1: 50-shot graph classification performance comparison with different pre-trained models. We color the **best** and **second best** models. The compared numbers of in-domain experiments are from EdgePrompt [Fu et al., 2025]. We only demonstrate the most competitive results reported in EdgePrompt here due to space limitations. Full comparison can be found in Appendix H.2.

Pre-training	Tuning Methods	ENZYMES	DD	NCI1	NCI109	Mutagenicity	Average
in-dataset	Classifier Only	27.07 \pm 1.04	61.77 \pm 2.40	61.27 \pm 3.64	62.12 \pm 1.10	67.36 \pm 0.71	55.92
	GraphPrompt [Liu et al., 2023b]	26.87 \pm 1.47	62.58 \pm 1.84	62.45 \pm 1.52	62.41 \pm 0.69	68.03 \pm 0.78	56.47
	ALL-in-one [Sun et al., 2023b]	25.73 \pm 1.18	65.16 \pm 1.47	58.52 \pm 1.59	62.01 \pm 0.66	64.43 \pm 1.00	55.17
	GPF [Fang et al., 2023]	28.53 \pm 1.76	65.64 \pm 0.70	61.45 \pm 3.13	61.90 \pm 1.26	67.19 \pm 0.74	56.94
	GPF-plus [Fang et al., 2023]	27.33 \pm 2.01	67.20 \pm 1.56	61.61 \pm 2.89	62.84 \pm 0.23	67.69 \pm 0.64	57.33
	EdgePrompt [Fu et al., 2025]	29.33 \pm 2.30	63.97 \pm 2.14	62.02 \pm 3.02	62.02 \pm 1.03	67.55 \pm 0.85	56.98
	EdgePrompt+ [Fu et al., 2025]	32.67 \pm 2.53	67.72 \pm 1.62	67.07 \pm 1.96	66.53 \pm 1.30	68.31 \pm 1.36	60.46
cross-dataset	GCN [Kipf and Welling, 2017]	43.33 \pm 1.05	65.84 \pm 2.77	61.36 \pm 2.00	62.17 \pm 0.66	60.46 \pm 1.75	58.63
	BRIDGE [Yuan et al., 2025a]	36.67 \pm 5.96	64.95 \pm 3.38	63.50 \pm 2.27	61.78 \pm 1.63	65.12 \pm 2.83	58.40
	GFT [Wang et al., 2024b]	34.61 \pm 3.12	56.00 \pm 1.77	59.16 \pm 6.25	60.50 \pm 2.71	67.82 \pm 3.18	55.61
	RiemannGFM [Sun et al., 2025]	34.27 \pm 1.72	68.74 \pm 1.31	55.10 \pm 2.24	59.86 \pm 1.30	62.56 \pm 4.04	56.11
GraphVec-FM		51.00 \pm 3.22	75.94 \pm 2.70	67.32 \pm 1.51	67.90 \pm 1.67	68.57 \pm 1.62	66.14
Unsupervised GraphVec-FM		48.33 \pm 2.36	74.02 \pm 1.26	66.11 \pm 2.30	64.34 \pm 2.38	68.38 \pm 2.88	64.23

4.7 Generalization Error Bound

Providing a theoretical guarantee for the generalization ability of GraphVec-FM, i.e., its performance on unseen test datasets, is crucial yet challenging, primarily due to the model's inherent complexity in both its objective and architectural design. Since the loss defined in (15) cannot intuitively reflect the model performance, we here consider a general metric learning loss $\ell \in [0, 1]$. An example is $\ell(G_u, G_v) = 1 - C_{uv} \cdot \zeta(\mathbf{g}_u, \mathbf{g}_v)$, where $C_{uv} = 1$ if G_u and G_v are in the same class and $C_{uv} = -1$ otherwise.

Theorem 4.2. Denote ϑ_1 the number of layers of each of the Q GINs, ϑ_2 the number of layers of the GT, κ_1 the MLP depth in each GIN, and κ_2 the MLP depth in the GT. Let \mathbf{W} be the weight matrix in a layer of the networks. Let $\tilde{\mathbf{Z}}$ be the whole input data matrix of the GINs and denote $\beta = \|\tilde{\mathbf{Z}}\|_F$. Let $\varsigma = \max_{(i,j) \in [N] \times [M]} \|\mathbf{A}_i^{(j)}\|_2$. Suppose ℓ is τ -Lipschitz continuous and the attention maps in GT are μ -Lipschitz continuous. Denote $\mathcal{L}(F) = \mathbb{E}_{G, G' \sim \mathbb{G}}[\ell(G, G')]$. Then with probability $1 - \delta$ over the training dataset \mathcal{D} , the following inequality holds

$$\mathcal{L}(F) \leq \frac{1}{MN(N-1)} \sum_{j=1}^M \sum_{u \neq v} \ell(G_u^{(j)}, G_v^{(j)}) + \frac{16 + 48\tau L_F \beta Q \bar{d} \sqrt{\ln(2Q\bar{d})} \ln(MN/2)}{MN} + \sqrt{\frac{\ln(1/\delta)}{2MN}}$$

where $L_F = \left(4\sqrt{\frac{\gamma R}{n}} + \frac{1}{\sqrt{n}}\right) \left(\varsigma^{\vartheta_1} \max_{q \in [Q]} \prod_{j=1}^{\kappa_1} \|\mathbf{W}_j^{GIN_q}\|_2\right) \left(\mu^{\vartheta_2} \prod_j^{\kappa_2} \|\mathbf{W}_j^{GT}\|_2\right)$.

The theorem has the following implications.

Table 2: Graph clustering performance on ENZYMES, NCI1, COLLAB, REDDIT-BINARY, REDDIT-MULTI. The comparison numbers are from AMGC [Yang et al., 2025].

Method	ENZYMES		NCI1		COLLAB		REDDIT-BINARY		REDDIT-MULTI	
	ACC	NMI	ACC	NMI	ACC	NMI	ACC	NMI	ACC	NMI
InfoGraph +KM	22.1 \pm 1.0	2.4 \pm 0.5	54.1 \pm 2.2	1.3 \pm 1.1	59.6 \pm 1.8	14.4 \pm 3.0	51.3 \pm 2.1	2.3 \pm 0.4	20.3 \pm 0.9	0.5 \pm 0.2
InfoGraph +SC	23.8 \pm 0.5	4.6 \pm 0.7	54.9 \pm 1.7	0.9 \pm 0.6	60.9 \pm 2.5	15.4 \pm 3.3	50.8 \pm 1.3	1.6 \pm 0.6	24.7 \pm 1.3	4.8 \pm 0.6
GraphCL +KM	21.5 \pm 0.2	1.6 \pm 0.1	55.4 \pm 1.7	0.5 \pm 0.3	58.0 \pm 1.2	17.8 \pm 2.0	51.9 \pm 3.3	3.4 \pm 1.2	25.3 \pm 0.9	5.3 \pm 0.3
GraphCL +SC	25.3 \pm 0.3	4.8 \pm 0.4	50.8 \pm 1.6	0.6 \pm 0.6	57.8 \pm 0.6	17.0 \pm 1.3	55.9 \pm 2.1	3.2 \pm 1.0	27.3 \pm 1.3	5.4 \pm 0.8
JOAO + KM	21.7 \pm 0.4	4.9 \pm 0.4	51.1 \pm 0.4	0.4 \pm 0.2	58.3 \pm 1.5	18.7 \pm 2.6	54.3 \pm 2.9	4.2 \pm 1.8	26.6 \pm 0.6	3.6 \pm 1.2
JOAO + SC	24.4 \pm 1.4	3.2 \pm 0.7	51.5 \pm 3.0	0.9 \pm 1.2	58.2 \pm 0.9	17.1 \pm 2.1	55.9 \pm 1.2	6.7 \pm 2.0	25.6 \pm 0.6	2.5 \pm 0.2
GLCC[Ju et al., 2023]	24.4 \pm 1.4	3.2 \pm 0.7	60.9 \pm 2.3	5.3 \pm 1.9	60.3 \pm 0.6	18.2 \pm 1.3	67.6 \pm 3.4	9.2 \pm 2.6	32.4 \pm 2.1	11.8 \pm 1.3
AMGC[Yang et al., 2025]	26.7 \pm 2.0	5.2 \pm 1.3	62.7 \pm 3.0	6.4 \pm 1.9	61.2 \pm 1.0	20.5 \pm 1.6	64.3 \pm 1.9	12.1 \pm 3.3	35.5 \pm 2.3	16.1 \pm 0.9
GraphVec-FM	29.1 \pm 0.4	7.7 \pm 0.3	64.8 \pm 0.0	6.5 \pm 0.0	61.8 \pm 0.0	21.2 \pm 0.0	71.6 \pm 0.0	20.7 \pm 0.0	40.0 \pm 0.2	17.3 \pm 0.1

- When the total number of training graphs MN is larger, the bound is tighter, which is further verified by the experiments in Figure 2. Note that if we use the unsupervised contrastive loss to train the model, due to the data augmentation (though the samples are not independent), the generalization could be stronger. That’s why in two cases of Table 3, the unsupervised learning outperformed the supervised learning.
- Although β often scales with \sqrt{n} , we have a factor $\frac{1}{\sqrt{n}}$ in L_F . This means that the number of nodes in each graph does not have a significant impact on the generalization, provided that the spectral norms of $\mathbf{A}_i^{(j)}$ increase slowly with n . As a result, our model will generalize well to both small graphs (e.g., ENZYMES) and large graphs (e.g., REDDIT), as shown by Tables 1 and 3.
- Since L_F scales with $\mathcal{O}(\sqrt{\gamma R})$, we could use a relatively large R to enrich the final vector representation for each graph, thereby improving the expressiveness. Moreover, L_F is not very sensitive to γ , which is learned adaptively.

5 Experiments

5.1 Few-Shot Graph Classification

Datasets and Baselines Following [Fu et al., 2025], we use five datasets from TUDataset [Morris et al., 2020], including ENZYMES, DD, NCI1, NCI109, and Mutagencity, to conduct few-shot graph classification experiments.

We evaluate our methods against baselines under two distinct settings:

1) In-dataset setting: In this setting, the training and testing sets are partitioned within the same dataset, and the model is fine-tuned using few-shot samples. We employ SimGRACE, [Xia et al., 2022], the most competitive pre-training strategy reported in EdgePrompt for pre-training and adopt seven different tuning mechanisms, including prompt-tuning methods such as GraphPrompt, All-In-One [Sun et al., 2023b], GPF [Fang et al., 2023], and GPF-plus [Fang et al., 2023], as well as standard classifier training.

2) Cross-dataset setting: This setting involves fine-tuning and testing on datasets that were unseen during the pre-training phase. Specifically, we adopt a leave-one-out strategy where each of the five datasets serves as the downstream target for testing, while the remaining four datasets are leveraged for pre-training. In cross domain setting we compared GraphVec-FM with 3 recent strong GFM baselines, GFT [Wang et al., 2024b], BRIDGE [Yuan et al., 2025a], and RiemannGFM [Sun et al., 2025], and 1 classic GNN [Kipf and Welling, 2017]. GraphVec-FM is pretrained and evaluated under this setting.

To further evaluate the transferability of GraphVec-FM in different domains, we conduct more experiments on 4 social network datasets, including COLLAB, REDDIT-BINARY, IMDB-BINARY, IMDB-MULTI and 3 computer vision datasets including Letter-med, COIL-RAG and Cuneiform using GraphVec-FM pre-trained on 5 bio-chemical datasets mentioned above. The results are compared with BRIDGE [Yuan et al., 2025a], ProNoG [Yu et al., 2025c] and EdgePrompt+ [Fu et al., 2025]. More details about the settings and datasets can be found in Appendix G.3 and G.1.

Results The results are reported in Table 1 and Table 3. As shown in Table 1, our GraphVec-FM consistently outperforms all baseline methods in the supervised pre-training paradigm and achieved second best in the unsupervised pre-training paradigm. Compared with in-domain baselines with different fine-tuning strategies under the cross-dataset setting, our model still achieves competitive performance. In social network and computer vision datasets that have a significant gap between pre-training datasets in both semantics and structure, our GraphVec-FM consistently outperforms other baselines. This performance demonstrates that our pre-trained model effectively learns generalizable

Table 3: Few-shot graph classification results on social network and computer vision datasets. 5-shot and 1-shot settings are adopted on COIL-RAG and Cuneiform, respectively due to a lack of enough samples in some classes.

Dataset	COLLAB 50-shot	REDDIT-B 50-shot	IMDB-B 50-shot	IMDB-M 50-shot	Letter-med 50-shot	COIL-RAG 5-shot	Cuneiform 1-shot
BRIDGE [Yuan et al., 2025a]	54.52 ± 3.73	57.80 ± 8.79	50.20 ± 6.27	36.6 ± 5.48	35.40 ± 2.09	27.02 ± 6.90	23.07 ± 9.42
ProNoG [Yu et al., 2025c]	46.88 ± 3.14	74.33 ± 2.05	60.8 ± 5.19	40.53 ± 0.66	56.98 ± 5.83	34.97 ± 7.62	10.00 ± 7.92
EdgePrompt+[Fu et al., 2025]	68.76 ± 1.60	74.60 ± 1.60	71.17 ± 1.07	46.60 ± 0.50	74.66 ± 1.69	5.60 ± 0.21	18.22 ± 0.72
GraphVec-FM	68.09 ± 2.99	81.52 ± 1.50	68.39 ± 4.06	46.70 ± 0.99	85.60 ± 1.44	74.20 ± 0.77	55.86 ± 8.15
Unsupervised GraphVec-FM	64.82 ± 1.87	80.62 ± 2.18	66.61 ± 1.66	45.00 ± 1.81	80.63 ± 1.87	72.22 ± 1.66	53.79 ± 5.97

graph embeddings across different domains without relying on delicately designed tuning methods. It also highlights the model’s capability to capture features from diverse domains while maintaining a strong generalization ability to new domains. Compared to the supervised pre-trained model, the unsupervised pre-trained model exhibits only a slight decrease in accuracy except for COLLAB and Letter-med. The unsupervised GraphVec-FM still outperforms all four baselines on 4 of the 7 datasets.

5.2 Graph Clustering

To further validate the superiority of our proposed model on graph-level tasks and quality of the graph embeddings obtained from GraphVec-FM, we conducted experiments on graph clustering: applying spectral clustering [Ng et al., 2001] to the graph representations produced by the pretrained model. As shown in Table 2, our methods perform best. The results validate the generalization ability of GraphVec-FM and the transferability of the graph embeddings obtained from the pretrained model on unseen domains and unseen structures.

Table 4: Resource consumption for large-scale dataset evaluation

Dataset	#Graphs	#Avg. Nodes	GPU Memory	RAM Memory	Wall Clock Time
COLOR-3	10500	61.31	2.08GB	23.17GB	626.84s
reddit_threads	203088	23.93	0.74GB	6.01GB	3139.53s

5.3 Scalability to Large-scale Dataset

The construction and decomposition of global multi-graphs become computationally intensive when the downstream dataset contains a large number of graphs and nodes. To ensure scalability, except for employing the Nyström approximation (mentioned in Section 4.1) to handle large graphs efficiently and reduce the complexity of kernel matrix operations, we also reduce the computation cost by splitting datasets into small batches and computing the mini-batch global graphs.

To further validate the scale ability during evaluation, we test the time and memory consumption to evaluate on two large datasets COLOR-3 and reddit_threads [Morris et al., 2020] with more than 10k graphs and 20k graphs respectively. For these experiments, each dataset is divided into blocks of 128 graphs to build the corresponding multi-graphs. The resulting resource usage is summarized in Table 4, demonstrating that the overhead remains manageable at this scale. Note that COLOR-3 exhibits higher GPU and RAM consumption compared to reddit_threads, primarily due to its larger average number of nodes.

More Results The extension to node classification task, 1/5/10/20-shot learning results, the impact of the number of pre-training datasets, more graph clustering results, full ablation study results, robustness evaluation on noisy input graphs, and time and memory consumption during pretraining are in Appendices H.3, H.6, H.5, H.8, H.10, H.11, and H.12 respectively.

6 Conclusions

This paper presented a graph foundation model trained on graph datasets from diverse domains. The model aims to represent graphs as vectors that are effective in graph-level downstream tasks. We introduced a multi-graph construction method to generate consistent node embeddings across different datasets and a reference distribution module to effectively utilize the information of node embeddings. The experiments of few-shot graph classification and graph clustering demonstrated the superiority of our method over the competitors. A limitation of GraphVec-FM is its inability

to perform zero-shot learning, as it does not leverage language models or any textual information. Future extension is to incorporate cross-modal alignment during training.

References

Aditya Grover and Jure Leskovec. node2vec: Scalable feature learning for networks. In *SIGKDD*, pages 855–864, 2016.

Hongyun Cai, Vincent W Zheng, and Kevin Chen-Chuan Chang. A comprehensive survey of graph embedding: Problems, techniques, and applications. *IEEE T-KDE*, 30(9):1616–1637, 2018.

Thomas N. Kipf and Max Welling. Semi-supervised classification with graph convolutional networks. In *International Conference on Learning Representations*, 2017. URL <https://openreview.net/forum?id=SU4ayYg1>.

Shiping Wang, Jinbin Yang, Jie Yao, Yang Bai, and William Zhu. An overview of advanced deep graph node clustering. *IEEE Transactions on Computational Social Systems*, 11(1):1302–1314, 2023.

Víctor Martínez, Fernando Berzal, and Juan-Carlos Cubero. A survey of link prediction in complex networks. *ACM computing surveys (CSUR)*, 49(4):1–33, 2016.

Johannes Kobler, Uwe Schöning, and Jacobo Torán. *The graph isomorphism problem: its structural complexity*. Springer Science & Business Media, 2012.

Fan-Yun Sun, Jordon Hoffman, Vikas Verma, and Jian Tang. Infograph: Unsupervised and semi-supervised graph-level representation learning via mutual information maximization. In *ICLR*, 2020.

Keyulu Xu, Weihua Hu, Jure Leskovec, and Stefanie Jegelka. How powerful are graph neural networks? In *ICLR*, 2019.

Jinyu Cai, Yunhe Zhang, Jicong Fan, Yali Du, and Wenzhong Guo. Dual contrastive graph-level clustering with multiple cluster perspectives alignment. In *Proceedings of the Thirty-Third International Joint Conference on Artificial Intelligence, IJCAI-24*, pages 3770–3779, 8 2024. Main Track.

Renjie Liao, Yujia Li, Yang Song, Shenlong Wang, Will Hamilton, David K Duvenaud, Raquel Urtasun, and Richard Zemel. Efficient graph generation with graph recurrent attention networks. *Advances in neural information processing systems*, 32, 2019.

Thomas Gärtner, Peter Flach, and Stefan Wrobel. On graph kernels: Hardness results and efficient alternatives. In *Learning Theory and Kernel Machines*, pages 129–143. Springer, 2003.

S Vichay N Vishwanathan, Nicol N Schraudolph, Risi Kondor, and Karsten M Borgwardt. Graph kernels. *JMLR*, 11: 1201–1242, 2010.

Nino Shervashidze, Pascal Schweitzer, Erik Jan Van Leeuwen, Kurt Mehlhorn, and Karsten M Borgwardt. Weisfeiler-lehman graph kernels. *JMLR*, 12(9), 2011.

Horst Bunke. On a relation between graph edit distance and maximum common subgraph. *Pattern recognition letters*, 18(8):689–694, 1997.

Zhiping Zeng, Anthony KH Tung, Jianyong Wang, Jianhua Feng, and Lizhu Zhou. Comparing stars: On approximating graph edit distance. *Proceedings of the VLDB Endowment*, 2(1):25–36, 2009.

Facundo Mémoli. Gromov–wasserstein distances and the metric approach to object matching. *Foundations of computational mathematics*, 11:417–487, 2011.

Jose Bento and Stratis Ioannidis. A family of tractable graph distances. In *Proceedings of the 2018 SIAM International Conference on Data Mining*, pages 333–341. SIAM, 2018.

Yan Sun and Jicong Fan. Mmd graph kernel: Effective metric learning for graphs via maximum mean discrepancy. In *ICLR*, 2024.

Yuning You, Tianlong Chen, Yongduo Sui, Ting Chen, Zhangyang Wang, and Yang Shen. Graph contrastive learning with augmentations. *Advances in Neural Information Processing Systems*, 33:5812–5823, 2020.

Yuning You, Tianlong Chen, Yang Shen, and Zhangyang Wang. Graph contrastive learning automated. In *ICML*, pages 12121–12132. PMLR, 2021.

Ziheng Sun, Chris Ding, and Jicong Fan. Lovász principle for unsupervised graph representation learning. In *Advances in Neural Information Processing Systems*, volume 36, pages 58290–58311. Curran Associates, Inc., 2023a.

Justin Gilmer, Samuel S Schoenholz, Patrick F Riley, Oriol Vinyals, and George E Dahl. Neural message passing for quantum chemistry. In *ICML*, pages 1263–1272. PMLR, 2017.

Zixiao Wang and Jicong Fan. Graph classification via reference distribution learning: Theory and practice. In *Advances in Neural Information Processing Systems*, volume 37, pages 137698–137740. Curran Associates, Inc., 2024.

Emiel Hoogeboom, Victor Garcia Satorras, Clément Vignac, and Max Welling. Equivariant diffusion for molecule generation in 3d. In *International conference on machine learning*, pages 8867–8887. PMLR, 2022.

Mikhail Galkin, Xinyu Yuan, Hesham Mostafa, Jian Tang, and Zhaocheng Zhu. Towards foundation models for knowledge graph reasoning. *arXiv preprint arXiv:2310.04562*, 2023.

Wenqing Zheng, Edward W Huang, Nikhil Rao, Zhangyang Wang, and Karthik Subbian. You only transfer what you share: Intersection-induced graph transfer learning for link prediction. *arXiv preprint arXiv:2302.14189*, 2023.

Haitao Mao, Zhikai Chen, Wenzhuo Tang, Jianan Zhao, Yao Ma, Tong Zhao, Neil Shah, Mikhail Galkin, and Jiliang Tang. Position: Graph foundation models are already here. In *Forty-first International Conference on Machine Learning*, 2024.

Jun Xia, Chengshuai Zhao, Bozhen Hu, Zhangyang Gao, Cheng Tan, Yue Liu, Siyuan Li, and Stan Z Li. Mole-bert: Rethinking pre-training graph neural networks for molecules. 2023.

Duo Zhang, Xinjian Liu, Xiangyu Zhang, Chengqian Zhang, Chun Cai, Hangrui Bi, Yiming Du, Xuejian Qin, Jiameng Huang, Bowen Li, et al. Dpa-2: Towards a universal large atomic model for molecular and material simulation. *arXiv preprint arXiv:2312.15492*, 2023.

Mikhail Galkin, Jincheng Zhou, Bruno Ribeiro, Jian Tang, and Zhaocheng Zhu. Zero-shot logical query reasoning on any knowledge graph. *arXiv preprint arXiv:2404.07198*, 2024.

Jianan Zhao, Hesham Mostafa, Michael Galkin, Michael Bronstein, Zhaocheng Zhu, and Jian Tang. Graphany: A foundation model for node classification on any graph. *arXiv preprint arXiv:2405.20445*, 2024a.

Divyansha Lachi, Mehdi Azabou, Vinam Arora, and Eva Dyer. Graphfm: A scalable framework for multi-graph pretraining. *arXiv preprint arXiv:2407.11907*, 2024.

Wenzhuo Tang, Haitao Mao, Danial Dervovic, Ivan Brugere, Saumitra Mishra, Yuying Xie, and Jiliang Tang. Cross-domain graph data scaling: A showcase with diffusion models. *arXiv preprint arXiv:2406.01899*, 2024a.

Zhilin Yang, William Cohen, and Ruslan Salakhudinov. Revisiting semi-supervised learning with graph embeddings. In *International conference on machine learning*, pages 40–48. PMLR, 2016.

Vijay Prakash Dwivedi, Chaitanya K Joshi, Anh Tuan Luu, Thomas Laurent, Yoshua Bengio, and Xavier Bresson. Benchmarking graph neural networks. *Journal of Machine Learning Research*, 24(43):1–48, 2023.

Bahare Fatemi, Jonathan Halcrow, and Bryan Perozzi. Talk like a graph: Encoding graphs for large language models. *arXiv preprint arXiv:2310.04560*, 2023.

Hao Liu, Jiarui Feng, Lecheng Kong, Ningyue Liang, Dacheng Tao, Yixin Chen, and Muhan Zhang. One for all: Towards training one graph model for all classification tasks. *arXiv preprint arXiv:2310.00149*, 2023a.

Jiabin Tang, Yuhao Yang, Wei Wei, Lei Shi, Lixin Su, Suqi Cheng, Dawei Yin, and Chao Huang. Graphgpt: Graph instruction tuning for large language models. In *Proceedings of the 47th International ACM SIGIR Conference on Research and Development in Information Retrieval*, pages 491–500, 2024b.

Heng Wang, Shangbin Feng, Tianxing He, Zhaoxuan Tan, Xiaochuang Han, and Yulia Tsvetkov. Can language models solve graph problems in natural language? *Advances in Neural Information Processing Systems*, 36, 2024a.

Jiawei Liu, Cheng Yang, Zhiyuan Lu, Junze Chen, Yibo Li, Mengmei Zhang, Ting Bai, Yuan Fang, Lichao Sun, Philip S Yu, et al. Graph foundation models: Concepts, opportunities and challenges. *IEEE Transactions on Pattern Analysis and Machine Intelligence*, 2025.

Yu Rong, Yatao Bian, Tingyang Xu, Weiyang Xie, Ying Wei, Wenbing Huang, and Junzhou Huang. Self-supervised graph transformer on large-scale molecular data. *NeurIPS*, 33:12559–12571, 2020.

Jiezhong Qiu, Qibin Chen, Yuxiao Dong, Jing Zhang, Hongxia Yang, Ming Ding, Kuansan Wang, and Jie Tang. Gcc: Graph contrastive coding for graph neural network pre-training. In *Proceedings of the 26th ACM SIGKDD international conference on knowledge discovery & data mining*, pages 1150–1160, 2020.

Xingtong Yu, Zechuan Gong, Chang Zhou, Yuan Fang, and Hui Zhang. Samgpt: Text-free graph foundation model for multi-domain pre-training and cross-domain adaptation. In *Proceedings of the ACM on Web Conference 2025*, pages 1142–1153, 2025a.

Xingbo Fu, Yinhai He, and Jundong Li. Edge prompt tuning for graph neural networks. In *The Thirteenth International Conference on Learning Representations*, 2025. URL <https://openreview.net/forum?id=92vMaHotTM>.

Xingtong Yu, Chang Zhou, Zhongwei Kuai, Xinming Zhang, and Yuan Fang. Gcot: Chain-of-thought prompt learning for graphs. *arXiv preprint arXiv:2502.08092*, 2025b.

Shuo Wang, Bokui Wang, Zhixiang Shen, Boyan Deng, and Zhao Kang. Multi-domain graph foundation models: Robust knowledge transfer via topology alignment. *arXiv preprint arXiv:2502.02017*, 2025a.

Wei Wei, Xubin Ren, Jiabin Tang, Qinyong Wang, Lixin Su, Suqi Cheng, Junfeng Wang, Dawei Yin, and Chao Huang. Llmrec: Large language models with graph augmentation for recommendation. In *Proceedings of the 17th ACM International Conference on Web Search and Data Mining*, pages 806–815, 2024.

Fan-Yun Sun, Jordan Hoffmann, Vikas Verma, and Jian Tang. Infograph: Unsupervised and semi-supervised graph-level representation learning via mutual information maximization. *arXiv preprint arXiv:1908.01000*, 2019.

Petar Veličković, William Fedus, William L Hamilton, Pietro Liò, Yoshua Bengio, and R Devon Hjelm. Deep graph infomax. In *ICLR*, 2019.

Jun Xia, Lirong Wu, Jintao Chen, Bozhen Hu, and Stan Z Li. Simgrace: A simple framework for graph contrastive learning without data augmentation. In *Proceedings of the ACM web conference 2022*, pages 1070–1079, 2022.

Haihong Zhao, Aochuan Chen, Xiangguo Sun, Hong Cheng, and Jia Li. All in one and one for all: A simple yet effective method towards cross-domain graph pretraining. In *Proceedings of the 30th ACM SIGKDD Conference on Knowledge Discovery and Data Mining*, pages 4443–4454, 2024b.

Zhenyu Hou, Xiao Liu, Yukuo Cen, Yuxiao Dong, Hongxia Yang, Chunjie Wang, and Jie Tang. Graphmae: Self-supervised masked graph autoencoders. In *Proceedings of the 28th ACM SIGKDD conference on knowledge discovery and data mining*, pages 594–604, 2022.

Zhenyu Hou, Yufei He, Yukuo Cen, Xiao Liu, Yuxiao Dong, Evgeny Kharlamov, and Jie Tang. Graphmae2: A decoding-enhanced masked self-supervised graph learner. In *Proceedings of the ACM web conference 2023*, pages 737–746, 2023.

Mingchen Sun, Kaixiong Zhou, Xin He, Ying Wang, and Xin Wang. Gppt: Graph pre-training and prompt tuning to generalize graph neural networks. In *Proceedings of the 28th ACM SIGKDD Conference on Knowledge Discovery and Data Mining*, pages 1717–1727, 2022.

Taoran Fang, Yunchao Zhang, Yang Yang, Chunping Wang, and Lei Chen. Universal prompt tuning for graph neural networks. *Advances in Neural Information Processing Systems*, 36:52464–52489, 2023.

Xiangguo Sun, Hong Cheng, Jia Li, Bo Liu, and Jihong Guan. All in one: Multi-task prompting for graph neural networks. In *Proceedings of the 29th ACM SIGKDD Conference on Knowledge Discovery and Data Mining*, pages 2120–2131, 2023b.

Zemin Liu, Xingtong Yu, Yuan Fang, and Xinming Zhang. Graphprompt: Unifying pre-training and downstream tasks for graph neural networks. In *Proceedings of the ACM web conference 2023*, pages 417–428, 2023b.

Haonan Yuan, Qingyun Sun, Junhua Shi, Xingcheng Fu, Bryan Hooi, Jianxin Li, and Philip S Yu. How much can transfer? bridge: Bounded multi-domain graph foundation model with generalization guarantees. In *Forty-second International Conference on Machine Learning*, 2025a.

Xingtong Yu, Jie Zhang, Yuan Fang, and Renhe Jiang. Non-homophilic graph pre-training and prompt learning. In *Proceedings of the 31st ACM SIGKDD Conference on Knowledge Discovery and Data Mining V. 1*, pages 1844–1854, 2025c.

Chuang Liu, Yibing Zhan, Jia Wu, Chang Li, Bo Du, Wenbin Hu, Tongliang Liu, and Dacheng Tao. Graph pooling for graph neural networks: Progress, challenges, and opportunities. *arXiv preprint arXiv:2204.07321*, 2022.

Andrew Ng, Michael Jordan, and Yair Weiss. On spectral clustering: Analysis and an algorithm. *NeurIPS*, 14, 2001.

Corinna Cortes and Vladimir Vapnik. Support-vector networks. *Machine Learning*, 20:273–297, 1995.

Christopher Williams and Matthias Seeger. Using the nyström method to speed up kernel machines. *Advances in neural information processing systems*, 13, 2000.

Rasmus Bro, Evrim Acar, and Tamara G Kolda. Resolving the sign ambiguity in the singular value decomposition. *Journal of Chemometrics: A Journal of the Chemometrics Society*, 22(2):135–140, 2008.

Emanuel Parzen. On estimation of a probability density function and mode. *The annals of mathematical statistics*, 33(3):1065–1076, 1962.

Ladislav Rampášek, Michael Galkin, Vijay Prakash Dwivedi, Anh Tuan Luu, Guy Wolf, and Dominique Beaini. Recipe for a general, powerful, scalable graph transformer. *Advances in Neural Information Processing Systems*, 35:14501–14515, 2022.

Arthur Gretton, Karsten M Borgwardt, Malte J Rasch, Bernhard Schölkopf, and Alexander Smola. A kernel two-sample test. *The Journal of Machine Learning Research*, 13(1):723–773, 2012.

Aaron van den Oord, Yazhe Li, and Oriol Vinyals. Representation learning with contrastive predictive coding. *arXiv preprint arXiv:1807.03748*, 2018.

Zehong Wang, Zheyuan Zhang, Nitesh Chawla, Chuxu Zhang, and Yanfang Ye. Gft: Graph foundation model with transferable tree vocabulary. *Advances in Neural Information Processing Systems*, 37:107403–107443, 2024b.

Li Sun, Zhenhao Huang, Suyang Zhou, Qiqi Wan, Hao Peng, and Philip Yu. Riemannngfm: Learning a graph foundation model from riemannian geometry. In *Proceedings of the ACM on Web Conference 2025*, pages 1154–1165, 2025.

Christopher Morris, Nils M. Kriege, Franka Bause, Kristian Kersting, Petra Mutzel, and Marion Neumann. Tudataset: A collection of benchmark datasets for learning with graphs. In *ICML 2020 Workshop on Graph Representation Learning and Beyond (GRL+ 2020)*, 2020. URL www.graphlearning.io.

Jinbin Yang, Jinyu Cai, Yunhe Zhang, Sujia Huang, and Shiping Wang. Towards adaptive masked structural learning for graph-level clustering. *IEEE Transactions on Network Science and Engineering*, 2025.

Wei Ju, Yiyang Gu, Binqi Chen, Gongbo Sun, Yifang Qin, Xingyuming Liu, Xiao Luo, and Ming Zhang. Glcc: A general framework for graph-level clustering. In *AAAI*, volume 37, pages 4391–4399, 2023.

Haonan Yuan, Qingyun Sun, Junhua Shi, Xingcheng Fu, Bryan Hooi, Jianxin Li, and Philip S Yu. Graver: Generative graph vocabularies for robust graph foundation models fine-tuning. *arXiv preprint arXiv:2511.05592*, 2025b.

Xingtong Yu, Chang Zhou, Yuan Fang, and Xinming Zhang. Multigprompt for multi-task pre-training and prompting on graphs. In *Proceedings of the ACM Web Conference 2024*, pages 515–526, 2024a.

Ben Finkelstein, İsmail İlkan Ceylan, Michael Bronstein, and Ron Levie. Equivariance everywhere all at once: A recipe for graph foundation models. *arXiv preprint arXiv:2506.14291*, 2025.

Xingliang Wang, Zemin Liu, Junxiao Han, and Shuguang Deng. Rag4gfm: Bridging knowledge gaps in graph foundation models through graph retrieval augmented generation. In *The Thirty-ninth Annual Conference on Neural Information Processing Systems*, 2025b.

Kai Wang and Siqiang Luo. Towards graph foundation models: The perspective of zero-shot reasoning on knowledge graphs. *arXiv e-prints*, pages arXiv–2410, 2024.

Jatin Chauhan, Deepak Nathani, and Manohar Kaul. Few-shot learning on graphs via super-classes based on graph spectral measures. In *International Conference on Learning Representations*.

Kaveh Hassani. Cross-domain few-shot graph classification. In *Proceedings of the AAAI Conference on Artificial Intelligence*, volume 36, pages 6856–6864, 2022.

Xingtong Yu, Zhenghao Liu, Yuan Fang, Zemin Liu, Sihong Chen, and Xinming Zhang. Generalized graph prompt: Toward a unification of pre-training and downstream tasks on graphs. *IEEE Transactions on Knowledge and Data Engineering*, 2024b.

Peter H Schönemann. A generalized solution of the orthogonal procrustes problem. *Psychometrika*, 31(1):1–10, 1966.

Colin McDiarmid et al. On the method of bounded differences. *Surveys in combinatorics*, 141(1):148–188, 1989.

Peter L Bartlett, Dylan J Foster, and Matus J Telgarsky. Spectrally-normalized margin bounds for neural networks. *Advances in neural information processing systems*, 30, 2017.

Diederik Kinga, Jimmy Ba Adam, et al. A method for stochastic optimization. In *International conference on learning representations (ICLR)*, volume 5. San Diego, California;, 2015.

Hongteng Xu, Jiachang Liu, Dixin Luo, and Lawrence Carin. Representing graphs via gromov-wasserstein factorization. *IEEE T-PAMI*, 2022.

A Notations

Symbol	Meaning	Symbol	Meaning
x	a real number	\mathbf{x}	a vector
\mathbf{X}	a matrix	\mathbf{I}_n	identity matrix of size $n \times n$
G	a graph	\mathbf{g}	vector representation of G
\mathcal{G}	a set of graphs	\mathcal{D}	a dataset
$\ \mathbf{x}\ $	the Euclidean norm of \mathbf{x}	$\ \mathbf{x}\ _1$	the ℓ_1 norm of \mathbf{x}
$[M]$	the set $\{1, 2, \dots, M\}$	$\mathbf{X} \ \mathbf{Y}$ or $[\mathbf{X}, \mathbf{Y}]$	vertical concatenation
$\ \mathbf{X}\ _F$	Frobenius norm of matrix	$\ \mathbf{X}\ _2$	spectral norm of matrix

Table 5: Notations

B More about Related Work

Language Model-Free GFMs Many studies have explored training GFMs using the “pre-train and adaptation” paradigm, leveraging message-passing-based or transformer-based GNNs as backbones. These approaches typically employ contrastive or generative self-supervised learning for pretraining, followed by fine-tuning a subset of model parameters to adapt to downstream tasks or datasets [Liu et al., 2025]. Contrastive methods [Qiu et al., 2020, Sun et al., 2019, Veličković et al., 2019, Xia et al., 2022] typically aim to produce generalized graph representations through maximizing the agreement between different augmentations of the same instance. For example, GraphCL [You et al., 2020] designs four types of graph data augmentations to learn invariant representations under specialized perturbations. GCOPE [Zhao et al., 2024b] employs a graph contrastive learning framework and introduces coordinators which are some virtual nodes that function as dynamic bridges between disparate graph datasets. Focused on node-level tasks, it effectively mitigates negative transfer effects when pretraining graph models on cross-domain datasets. In the meantime, generative methods pre-train GNNs through graph reconstruction or property prediction. For instance, GraphMAEs [Hou et al., 2022, 2023] employed the reconstruction of features with masking strategies. Recently, graph prompt tuning methods [Sun et al., 2022, Fang et al., 2023, Sun et al., 2023b, Liu et al., 2023b] have been proposed as an adaptation mechanism to bridge the gap between pretraining tasks and downstream tasks. GraphPrompt [Liu et al., 2023b] converts the pre-training task and downstream tasks to follow the same template based on subgraph similarity and uses learnable prompt vectors to implement different aggregation schemes for readout in different downstream tasks. EdgePrompt [Fu et al., 2025] manipulates input graphs by learning prompt vectors for edges and incorporates the edge prompts through message passing in the pre-trained GNN models. As an effective adaptation mechanism, these methods have been widely adopted in subsequent GFMs [Yuan et al., 2025a,b, Wang et al., 2025a, Yu et al., 2024a, 2025a]. Recently, several notable Graph Foundation Models have been introduced. RiemannGFM [Sun et al., 2025] embeds nodes into a Riemann manifold using structural vocabulary of trees as circles, enable structural transferability across domains. TS-GNN [Finkelshtein et al., 2025] investigates symmetries that a graph foundation model must respect, which is mainly designed for node-level tasks. RAG4GFM [Wang et al., 2025b] applies the Retrieval-Augmented Generation (RAG) paradigm to Graph Foundation Models, allowing them to dynamically access and integrate graph knowledge at inference time. SCORE [Wang and Luo, 2024] utilizes KGs as a unified topological structure to tackle diverse tasks.

LLM-based GFMs These models utilize the strong capacity of large language models to conduct graph analysis. For instance, GraphQA [Fatemi et al., 2023] converts graph connectivity into textual descriptions and uses LLMs to answer graph reasoning questions. By enriching these prompts with domain-specific context, GraphQA can effectively learn cross-domain structural representations, essentially serving as a structural GFM. Similar approaches include NLGraph [Wang et al., 2024a], which tackles tasks like shortest path finding by translating graphs into text, demonstrating another viable pathway for unified structure learning. For unifying node feature representations, the One For All (OFA) framework [Liu et al., 2023a] offers an innovative solution. It aggregates diverse graph datasets into a unified text-attributed graph (TAG) format, then leverages LLMs to jointly learn feature representations that transcend domain boundaries. This approach effectively bridges the gap between heterogeneous graph data sources.

GFM for Graph-Level Tasks As mentioned before, most of the existing GFMs are designed for node-level tasks. There are a few studies that focus on graph-level tasks across domains. For instance, Chauhan et al. tries to pretrain GNNs on certain classes of a dataset and conduct few-shot classification on the remaining classes within the same dataset. Hassani [2022] adopts a meta-learning approach to learn model initialization for few-shot graph classification. These graph-level models are usually small and not general. Some GFMs can be adapted to graph-level tasks. For

instance, GraphPrompt [Liu et al., 2023b], GraphPrompt+ [Yu et al., 2024b], and EdgePrompt [Fu et al., 2025] use learnable prompts to adjust graph-level pooling for obtaining domain-adaptive graph embeddings. Other works such as SAMGPT [Yu et al., 2025a], ProNoG [Yu et al., 2025c] MultiGPrompt [Yu et al., 2024a], and BRIDGE [Yuan et al., 2025a] are also designed to effectively perform graph classification, but they mainly build on well-designed node embedding and use simple global pooling to apply the model to graph-level tasks.

C Derivation of Algorithm 1

Recall that we want to solve

$$\underset{\mathbf{R}_j \in \mathcal{R}, j \in [M]}{\text{maximize}} \frac{1}{M} \sum_{i=1}^M \sum_{j=1}^M \exp(-\gamma \|\mathbf{R}_i \boldsymbol{\mu}_i - \mathbf{R}_j \boldsymbol{\mu}_j\|^2) \triangleq \mathcal{L}(\{\mathbf{R}_j\}_{j=1}^M) \quad (17)$$

For convenience, we let $R := \{\mathbf{R}_j \in \mathcal{R}\}_{j \in [M]}$. It follows that

$$\begin{aligned} & \underset{R}{\text{maximize}} \sum_i \sum_j \exp(-\gamma \|\mathbf{R}_i \boldsymbol{\mu}_i - \mathbf{R}_j \boldsymbol{\mu}_j\|^2) \\ &= \underset{R}{\text{maximize}} \sum_i \sum_j \exp(-\gamma (\|\boldsymbol{\mu}_i\|^2 + \|\boldsymbol{\mu}_j\|^2)) \exp(2\gamma \langle \mathbf{R}_i \boldsymbol{\mu}_i, \mathbf{R}_j \boldsymbol{\mu}_j \rangle) \\ &= \underset{R}{\text{maximize}} \sum_i \sum_j w_{ij} \exp(2\gamma \langle \mathbf{R}_i \boldsymbol{\mu}_i, \mathbf{R}_j \boldsymbol{\mu}_j \rangle) \triangleq L(R) \end{aligned} \quad (18)$$

where $w_{ij} := \exp(-\gamma (\|\boldsymbol{\mu}_i\|^2 + \|\boldsymbol{\mu}_j\|^2))$. Let $R^{(t-1)}$ be the decision variables at iteration $t-1$. We introduce the first-order approximation of $L(R)$ at $R^{(t-1)}$ as follows:

$$\begin{aligned} \hat{L}(R) &:= \sum_i \sum_j w_{ij} \exp\left(2\gamma \langle \mathbf{R}_i^{(t-1)} \boldsymbol{\mu}_i, \mathbf{R}_j^{(t-1)} \boldsymbol{\mu}_j \rangle\right) \\ &\quad + \sum_i \left\langle 4\gamma \sum_j w_{ij} \exp\left(2\gamma \langle \mathbf{R}_i^{(t-1)} \boldsymbol{\mu}_i, \mathbf{R}_j^{(t-1)} \boldsymbol{\mu}_j \rangle\right) \mathbf{R}_j^{(t-1)} \boldsymbol{\mu}_j \boldsymbol{\mu}_i^\top, \mathbf{R}_i - \mathbf{R}_i^{(t-1)} \right\rangle \\ &= \sum_i \sum_j w_{ij} k_{ij}^{(t-1)} + 4\gamma \sum_i \left\langle \sum_j w_{ij} k_{ij}^{(t-1)} \mathbf{R}_j^{(t-1)} \boldsymbol{\mu}_j \boldsymbol{\mu}_i^\top, \mathbf{R}_i - \mathbf{R}_i^{(t-1)} \right\rangle \end{aligned} \quad (19)$$

where $k_{ij}^{(t-1)} := \exp\left(2\gamma \langle \mathbf{R}_i^{(t-1)} \boldsymbol{\mu}_i, \mathbf{R}_j^{(t-1)} \boldsymbol{\mu}_j \rangle\right)$. Since $L(R)$ is a convex function, it follows that

$$L(R) \geq \hat{L}(R) \quad (20)$$

It follows that

$$L(R) \geq \hat{L}(R) - 2\gamma \eta \sum_i \|\mathbf{R}_i - \mathbf{R}_i^{(t-1)}\|_F^2 \triangleq \bar{L}(R) \quad (21)$$

It means $\bar{L}(R)$ is a lower bound of $L(R)$. Therefore, instead of $L(R)$, we propose to maximize $\bar{L}(R)$:

$$\begin{aligned} & \underset{R}{\text{maximize}} \sum_i \sum_j w_{ij} k_{ij}^{(t-1)} + 4\gamma \sum_i \left\langle \sum_j w_{ij} k_{ij}^{(t-1)} \mathbf{R}_j^{(t-1)} \boldsymbol{\mu}_j \boldsymbol{\mu}_i^\top, \mathbf{R}_i - \mathbf{R}_i^{(t-1)} \right\rangle \\ &\quad - 2\gamma \eta \sum_i \|\mathbf{R}_i - \mathbf{R}_i^{(t-1)}\|_F^2 \\ &= \underset{R}{\text{maximize}} \sum_i \left\langle 4\gamma \sum_j w_{ij} k_{ij}^{(t-1)} \mathbf{R}_j^{(t-1)} \boldsymbol{\mu}_j \boldsymbol{\mu}_i^\top, \mathbf{R}_i - \mathbf{R}_i^{(t-1)} \right\rangle + 4\gamma \eta \sum_i \langle \mathbf{R}_i^{(t-1)}, \mathbf{R}_i \rangle \\ &= \underset{R}{\text{maximize}} \sum_i \left\langle \sum_j w_{ij} k_{ij}^{(t-1)} \mathbf{R}_j^{(t-1)} \boldsymbol{\mu}_j \boldsymbol{\mu}_i^\top + \eta \mathbf{R}_i^{(t-1)}, \mathbf{R}_i - \mathbf{R}_i^{(t-1)} \right\rangle \\ &= \underset{R}{\text{maximize}} \sum_i \langle \mathbf{H}_i^t, \mathbf{R}_i \rangle \end{aligned} \quad (22)$$

where $\mathbf{H}_i^{(t)} := \sum_j w_{ij} k_{ij}^{(t-1)} \mathbf{R}_j^{(t-1)} \boldsymbol{\mu}_j \boldsymbol{\mu}_j^\top + \eta \mathbf{R}_i^{(t-1)}$. This is the well-known orthogonal Procrustes problem [Schöenemann, 1966]. The optimal solution for each \mathbf{R}_i is

$$\mathbf{R}_i^t = \mathbf{U}_i \mathbf{V}_i^\top \quad (23)$$

where \mathbf{U}_i and \mathbf{V}_i are from the SVD of \mathbf{H}_i^t , i.e., $\mathbf{H}_i^t = \mathbf{U}_i \mathbf{S}_i \mathbf{V}_i^\top$.

D Proof for Theorem 4.1

Proof. According to the definition of $\bar{L}(R)$, we have

$$\bar{L}(R^{(t-1)}) = L(R^{(t-1)}) \quad (24)$$

At iteration t , since (23) provides the optimal solution to maximize $\bar{L}(R)$, we have

$$\bar{L}(R^{(t)}) \geq \bar{L}(R) \quad (25)$$

which holds for any R . Letting $R = R^{(t-1)}$ and using (24), we have

$$\hat{L}(R^{(t)}) - 2\gamma\eta \sum_i \|\mathbf{R}_i - \mathbf{R}_i^{(t-1)}\|_F^2 \geq \bar{L}(R^{(t-1)}) = L(R^{(t-1)}) \quad (26)$$

which means

$$\hat{L}(R^{(t)}) \geq L(R^{(t-1)}) + 2\gamma\eta \sum_i \|\mathbf{R}_i - \mathbf{R}_i^{(t-1)}\|_F^2 \quad (27)$$

According to (20), we have

$$\hat{L}(R^{(t)}) \leq L(R^{(t)}) \quad (28)$$

Now combining (27) and (28), we arrive at

$$L(R^{(t)}) \geq L(R^{(t-1)}) + 2\gamma\eta \sum_i \|\mathbf{R}_i - \mathbf{R}_i^{(t-1)}\|_F^2 \quad (29)$$

This means the objective function is non-decreasing. Summing up both sides of (29) from 1 to t , we obtain

$$L(R^{(t)}) \geq L(R^{(0)}) + 2\gamma\eta \sum_i \|\mathbf{R}_i - \mathbf{R}_i^{(t-1)}\|_F^2 \quad (30)$$

Since $L(R^{(t)}) < \infty$ and $L(R^{(0)}) > -\infty$, we obtain $2\gamma\eta \sum_i \|\mathbf{R}_i - \mathbf{R}_i^{(t-1)}\|_F^2 < \infty$. As $\gamma < 0$ and $\rho > 0$, we conclude that $\sum_i \|\mathbf{R}_i - \mathbf{R}_i^{(t-1)}\|_F^2 < \infty$. That means, when $t \rightarrow \infty$, $\mathbf{R}_i - \mathbf{R}_i^{(t-1)} \rightarrow \mathbf{0}$. The $\mathbf{R}_i^{(t)}$ is convergent, $\forall i \in [M]$. \square

E Proof for Theorem 4.2

Since (15) does not explicitly show the error related to classification or metric learning, here we consider the following pair-wise loss function ℓ instead. An example is as

$$\ell(G_u, G_v) = 1 - C_{uv} \cdot \zeta(\mathbf{g}_u, \mathbf{g}_v) \quad (31)$$

where $\zeta(\mathbf{g}_u, \mathbf{g}_v) = \frac{\mathbf{g}_u^\top \mathbf{g}_v}{\|\mathbf{g}_u\| \|\mathbf{g}_v\|}$ and $C_{uv} = 1$ if G_u and G_v are in the same class and $C_{uv} = -1$ if they are in different classes. Note that $\mathbf{g} = F(G)$, where $F \in \mathcal{F}$. The empirical risk is

$$\hat{\mathcal{L}}_{\mathcal{D}}(F) = \frac{1}{M} \sum_{j=1}^M \frac{1}{N(N-1)} \sum_{u \neq v} \ell(G_u^{(j)}, G_v^{(j)}) \triangleq \frac{1}{M} \sum_{j=1}^M \bar{\mathcal{L}}_{G_j}(F) \quad (32)$$

where we have assumed $N_1 = N_2 = \dots = N_M = N$ for convenience and $\bar{\mathcal{L}}_{G_j}(F) = \frac{1}{N(N-1)} \sum_{u \neq v} \ell(G_u^{(j)}, G_v^{(j)})$. The true risk is

$$\mathcal{L}(F) = \mathbb{E}_{G, G' \sim \mathbb{G}} [\ell(G, G')] \quad (33)$$

We would like to bound

$$\sup_{F \in \mathcal{F}} \{\hat{\mathcal{L}}_{\mathcal{D}}(F) - \mathcal{L}(F)\} \quad (34)$$

For any $\mathcal{D} = \{\mathcal{G}_1, \dots, \mathcal{G}_j, \dots, \mathcal{G}_M\}$ and $\tilde{\mathcal{D}} = \{\mathcal{G}_1, \dots, \tilde{\mathcal{G}}_j, \dots, \mathcal{G}_M\}$, where $\mathcal{G}_j = \{G_1^{(j)}, \dots, G_i^{(j)}, \dots, G_N^{(j)}\}$ and $\tilde{\mathcal{G}}_j = \{G_1^{(j)}, \dots, \tilde{G}_i^{(j)}, \dots, G_N^{(j)}\}$, we have

$$\begin{aligned}
& \left| \sup_{F \in \mathcal{F}} \{\hat{\mathcal{L}}_{\mathcal{D}}(F) - \mathcal{L}(F)\} - \sup_{F \in \mathcal{F}} \{\hat{\mathcal{L}}_{\tilde{\mathcal{D}}}(F) - \mathcal{L}(F)\} \right| \\
& \leq \sup_{F \in \mathcal{F}} \left| \hat{\mathcal{L}}_{\mathcal{D}}(F) - \hat{\mathcal{L}}_{\tilde{\mathcal{D}}}(F) \right| \\
& = \sup_{F \in \mathcal{F}} \left| \frac{1}{MN(N-1)} \left(\sum_{\mathcal{G}_j: u \neq v} \ell(G_u^{(j)}, G_v^{(j)}) - \sum_{\tilde{\mathcal{G}}_j: u \neq v} \ell(G_u^{(j)}, G_v^{(j)}) \right) \right| \\
& \leq \sup_{F \in \mathcal{F}} \left| \frac{1}{MN(N-1)} \left(\sum_{v \neq i} \left(\ell(G_i^{(j)}, G_v^{(j)}) - \ell(\tilde{G}_i^{(j)}, G_v^{(j)}) \right) \right) \right| \\
& \leq \sup_{F \in \mathcal{F}} \left| \frac{1}{MN(N-1)} \left(\sum_{v \neq i} \left| \ell(G_i^{(j)}, G_v^{(j)}) - \ell(\tilde{G}_i^{(j)}, G_v^{(j)}) \right| \right) \right| \\
& \leq \frac{1}{MN}
\end{aligned} \tag{35}$$

where the last inequality holds due to that $0 \leq \ell \leq 1$. Applying the McDiarmid's inequality (Lemma E.1) to $\sup_{F \in \mathcal{F}} \{\hat{\mathcal{L}}_{\mathcal{D}}(F) - \mathcal{L}(F)\}$, with probability at least $1 - \delta$, we have

$$\sup_{F \in \mathcal{F}} \{\hat{\mathcal{L}}_{\mathcal{D}}(F) - \mathcal{L}(F)\} \leq \mathbb{E}_{\mathcal{D}} \left(\sup_{F \in \mathcal{F}} \{\hat{\mathcal{L}}_{\mathcal{D}}(F) - \mathcal{L}(F)\} \right) + \sqrt{\frac{\ln(1/\delta)}{2MN}} \tag{36}$$

For convenience, we let $\bar{\ell}(G_u, G_v) = \ell(G_u, G_v) - \mathcal{L}(F)$, we have the following derivation

$$\begin{aligned}
& \mathbb{E}_{\mathcal{D}} \left(\sup_{F \in \mathcal{F}} \frac{1}{M} \sum_{j=1}^M \frac{1}{N(N-1)} \sum_{u \neq v} \bar{\ell}(G_u^{(j)}, G_v^{(j)}) \right) \\
& = \mathbb{E}_{\mathcal{D}} \left(\sup_{F \in \mathcal{F}} \frac{1}{M} \sum_{j=1}^M \frac{1}{N!} \sum_{\pi} \frac{1}{\lfloor N/2 \rfloor} \sum_{i=1}^{\lfloor N/2 \rfloor} \bar{\ell}(G_{\pi(i)}^{(j)}, G_{\pi(\lfloor N/2 \rfloor+i)}^{(j)}) \right) \\
& \leq \mathbb{E}_{\mathcal{D}} \left(\frac{1}{N!} \sum_{\pi} \sup_{F \in \mathcal{F}} \frac{1}{M} \sum_{j=1}^M \frac{1}{\lfloor N/2 \rfloor} \sum_{i=1}^{\lfloor N/2 \rfloor} \bar{\ell}(G_{\pi(i)}^{(j)}, G_{\pi(\lfloor N/2 \rfloor+i)}^{(j)}) \right) \\
& \leq \frac{1}{N!} \sum_{\pi} \mathbb{E}_{\mathcal{D}} \left(\sup_{F \in \mathcal{F}} \frac{1}{M} \sum_{j=1}^M \frac{1}{\lfloor N/2 \rfloor} \sum_{i=1}^{\lfloor N/2 \rfloor} \bar{\ell}(G_{\pi(i)}^{(j)}, G_{\pi(\lfloor N/2 \rfloor+i)}^{(j)}) \right) \\
& = \mathbb{E}_{\mathcal{D}} \left(\sup_{F \in \mathcal{F}} \frac{1}{M} \sum_{j=1}^M \frac{1}{\lfloor N/2 \rfloor} \sum_{i=1}^{\lfloor N/2 \rfloor} \bar{\ell}(G_{\pi(i)}^{(j)}, G_{\pi(\lfloor N/2 \rfloor+i)}^{(j)}) \right) \\
& = \mathbb{E}_{\mathcal{D}} \left(\sup_{F \in \mathcal{F}} \left\{ \tilde{\mathcal{L}}_{\mathcal{D}}(F) - \mathcal{L}(F) \right\} \right)
\end{aligned} \tag{37}$$

where $\tilde{\mathcal{L}}_{\mathcal{D}}(F) = \frac{1}{M} \sum_{j=1}^M \frac{1}{\lfloor N/2 \rfloor} \sum_{i=1}^{\lfloor N/2 \rfloor} \ell(G_{\pi(i)}^{(j)}, G_{\pi(\lfloor N/2 \rfloor+i)}^{(j)})$.

For convenience, we let $S = M \lfloor N/2 \rfloor$ and rename the graph-pair as (G_s, \bar{G}_s) . So we have S independent samples. By introducing a virtual dataset $\mathcal{D}' \subset \mathbb{G}$ with size S , we obtain

$$\begin{aligned}
& \mathbb{E}_{\mathcal{D}} \left(\sup_{F \in \mathcal{F}} \left\{ \tilde{\mathcal{L}}_{\mathcal{D}}(F) - \mathcal{L}(F) \right\} \right) \\
&= \mathbb{E}_{\mathcal{D}} \left(\sup_{F \in \mathcal{F}} \left\{ \frac{1}{S} \sum_{s=1}^S \ell(G_s, \bar{G}_s) - \mathcal{L}(F) \right\} \right) \\
&= \mathbb{E}_{\mathcal{D}} \left(\sup_{F \in \mathcal{F}} \left\{ \frac{1}{S} \sum_{s=1}^S \ell(G_s, \bar{G}_s) - \mathbb{E}_{\mathcal{D}'} \left(\frac{1}{S} \sum_{s=1}^S \ell(G'_s, \bar{G}'_s) \right) \right\} \right) \\
&\leq \mathbb{E}_{\mathcal{D}, \mathcal{D}'} \left(\sup_{F \in \mathcal{F}} \frac{1}{S} \sum_{s=1}^S [\ell(G_s, \bar{G}_s) - \ell(G'_s, \bar{G}'_s)] \right)
\end{aligned} \tag{38}$$

where the inequality holds due to Jensen's inequality. By introducing the Rademacher variable $\epsilon_s \in \{-1, 1\}$, we have

$$\begin{aligned}
& \mathbb{E}_{\mathcal{D}} \left(\sup_{F \in \mathcal{F}} \left\{ \tilde{\mathcal{L}}_{\mathcal{D}}(F) - \mathcal{L}(F) \right\} \right) \\
&\leq \mathbb{E}_{\mathcal{D}, \mathcal{D}'} \mathbb{E}_{\epsilon} \left(\sup_{F \in \mathcal{F}} \frac{1}{S} \sum_{s=1}^S \epsilon_s [\ell(G_s, \bar{G}_s) - \ell(G'_s, \bar{G}'_s)] \right) \\
&\leq \mathbb{E}_{\mathcal{D}, \mathcal{D}'} \mathbb{E}_{\epsilon} \left(\sup_{F \in \mathcal{F}} \left\{ \frac{1}{S} \sum_{s=1}^S \epsilon_s \ell(G_s, \bar{G}_s) \right\} + \sup_{F \in \mathcal{F}} \left\{ \frac{1}{S} \sum_{s=1}^S (-\epsilon_s) (G'_s, \bar{G}'_s) \right\} \right) \\
&\leq 2 \mathbb{E}_{\mathcal{D}, \epsilon} \left(\sup_{F \in \mathcal{F}} \frac{1}{S} \sum_{s=1}^S \epsilon_s \ell(G_s, \bar{G}_s) \right) \\
&= 2 \mathbb{E}_S(\hat{\mathcal{R}}_S(\mathcal{F}))
\end{aligned} \tag{39}$$

where $\mathcal{R}_S(\mathcal{F}) := \mathbb{E}_S(\hat{\mathcal{R}}_S(\mathcal{F}))$ is the Rademacher complexity.

Combining (36), we arrive at

$$\sup_{F \in \mathcal{F}} \{\hat{\mathcal{L}}_{\mathcal{D}}(F) - \mathcal{L}(F)\} \leq 2\mathcal{R}_S(\mathcal{F}) + \sqrt{\frac{\ln(1/\delta)}{2MN}} \tag{40}$$

According to Lemma E.4, Lemma E.5, and Lemma E.6, the Lipschitz constants of the GIN, GT, and reference layer are

$$\begin{aligned}
L_{\text{GIN}} &= \max_{(i,p) \in [N] \times [M]} \|\mathbf{A}_i^{(p)}\|_2^{\vartheta} \prod_{j=1}^{\vartheta'} \|\mathbf{W}_j\|_2 \\
L_{\text{Ref}} &= 4\sqrt{\frac{\gamma R}{n}} \\
L_{\text{GT}} &= \mu^{\vartheta} \prod_{j=1}^{\vartheta \vartheta'} \|\mathbf{W}_j\|_2
\end{aligned} \tag{41}$$

Since there are Q parallel GINs, according to Lemma E.8, the Lipschitz constant of their combinations is

$$L_{\text{QGIN}} = \max_q L_{\text{GIN}}^{(q)} \tag{42}$$

where $L_{\text{GIN}}^{(q)} = \max_{(i,p) \in [N] \times [M]} \|\mathbf{A}_i^{(p)}\|_2^{\vartheta} \prod_{j=1}^{\vartheta'} \|\mathbf{W}_j^{(q)}\|_2$. Based on the composition of these network components and their specific configurations, the Lipschitz constant of F is

$$L_F = \left(4\sqrt{\frac{\gamma R}{n}} + \frac{1}{\sqrt{n}} \right) \left(\max_{(i,p) \in [N] \times [M]} \|\mathbf{A}_i^{(p)}\|_2^{\vartheta_1} \max_{q \in [Q]} \prod_{j=1}^{\kappa_1} \|\mathbf{W}_j^{\text{GIN}_q}\|_2 \right) \left(\mu^{\vartheta_2} \prod_j^{\kappa_2} \|\mathbf{W}_j^{\text{GT}}\|_2 \right) \tag{43}$$

where κ_1 is the maximum number of MLP layers in each GIN and κ_2 is the total number of weight matrices excluding those in the attention maps of the transformer. Suppose the loss function ℓ is τ -Lipschitz, then the Lipschitz constant of $\ell \circ \mathcal{F}$ is $L_{\ell \circ \mathcal{F}} = \tau L_F$.

Let $\tilde{\mathbf{Z}}^{(j)} = [\bar{\mathbf{A}}^{(j)} \mathbf{Z}_1^{(j)}, \dots, \bar{\mathbf{A}}^{(j)} \mathbf{Z}_Q^{(j)}]$, where $\bar{\mathbf{A}}^{(j)} = \text{diag}(\mathbf{A}_1^{(j)}, \dots, \mathbf{A}_N^{(j)}) \in \mathbb{R}^{Nn \times Nn}$. We further form $\hat{\mathbf{Z}} = [\tilde{\mathbf{Z}}^{(1)}; \tilde{\mathbf{Z}}^{(2)}; \dots; \tilde{\mathbf{Z}}^{(M)}] \in \mathbb{R}^{MNn \times Q\bar{d}}$. According to Lemma E.7, the covering number of $\mathcal{Z} = \{\hat{\mathbf{Z}} \in \mathbb{R}^{MNn \times Q\bar{d}} : \|\hat{\mathbf{Z}}\|_F \leq \beta\}$ is bounded as

$$\ln \mathcal{N}(\mathcal{Z}, \epsilon, \|\cdot\|_F) \leq \frac{\beta^2 Q^2 \bar{d}^2 \ln(2Q\bar{d})}{\epsilon^2} \quad (44)$$

Therefore, using Lemma E.9, the covering number of $\ell \circ \mathcal{F} \times \mathcal{Z}$ is bounded as

$$\ln \mathcal{N}(\ell \circ \mathcal{F}, \epsilon, \|\cdot\|_F) \leq \frac{\tau^2 L_F^2 \beta^2 Q^2 \bar{d}^2 \ln(2Q\bar{d})}{\epsilon^2} \triangleq \frac{\varphi}{\epsilon^2} \quad (45)$$

Using Lemma E.2, we can bound the Rademacher complexity of our model class as

$$\begin{aligned} \mathcal{R}_S(\ell \circ \mathcal{F}) &\leq \inf_{\alpha > 0} \left(\frac{4\alpha}{\sqrt{S}} + \frac{12}{S} \int_{\alpha}^{\sqrt{S}} \frac{\sqrt{\varphi}}{\epsilon} d\epsilon \right) \\ &\leq \inf_{\alpha > 0} \left(\frac{4\alpha}{\sqrt{S}} + \frac{12\sqrt{\varphi}}{S} \ln\left(\frac{\sqrt{S}}{\alpha}\right) \right) \\ &\leq \frac{4 + 12\sqrt{\varphi} \ln(S)}{S} \end{aligned} \quad (46)$$

where in the last inequality we have let $\alpha = 1/\sqrt{S}$.

Now combining (46), (45), and (40), we arrive at

$$\hat{\mathcal{L}}_{\mathcal{D}}(F) \leq \mathcal{L}(F) + \frac{16 + 48\tau L_F \beta Q \bar{d} \sqrt{\ln(2Q\bar{d})} \ln(MN/2)}{MN} + \sqrt{\frac{\ln(1/\delta)}{2MN}} \quad (47)$$

This completes the proof.

E.1 Supporting Lemmas and Their Proofs

Lemma E.1 (McDiarmid's inequality [McDiarmid et al., 1989]). *Suppose $f : \prod_{k=1}^m \Omega_k \rightarrow \mathbb{R}$ with bounded differences $\{c_k\}_{k=1}^m$ then, for all $\epsilon > 0$, there holds*

$$\Pr_{\mathbf{z}} \{f(\mathbf{z}) - \mathbb{E}_{\mathbf{z}} f(\mathbf{z}) \geq \epsilon\} \leq e^{-\frac{2\epsilon^2}{\sum_{k=1}^m c_k^2}}$$

Lemma E.2. *Suppose the Lipschitz constant of $\ell \circ F$ is L , then the Rademacher complexity of $\ell \circ \mathcal{F}$ is bound as*

$$\mathcal{R}_S(\ell \circ \mathcal{F}) \leq \text{xxx} \quad (48)$$

Proof. We show the Dudley entropy integral bound Bartlett et al. [2017] below.

Lemma E.3. *Let \mathcal{F} be a real-valued function class taking values in $[0, 1]$, and assume that $\mathbf{0} \in \mathcal{F}$. Then*

$$\mathcal{R}_S(\mathcal{F}) \leq \inf_{\alpha > 0} \left(\frac{4\alpha}{\sqrt{S}} + \frac{12}{S} \int_{\alpha}^{\sqrt{S}} \sqrt{\ln \mathcal{N}(\epsilon, \mathcal{F}, \rho)} d\epsilon \right).$$

□

Lemma E.4. *The Lipschitz constant of the reference layer is $L_{\text{ref}} = 4\sqrt{\frac{\theta R}{n}}$.*

Proof. According to the definition of MMD, we have

$$\begin{aligned}
|\text{MMD}^2(\mathbf{H}, \mathbf{V}) - \text{MMD}^2(\mathbf{H}', \mathbf{V})| &\leq \left| \frac{1}{n^2} \sum_{i,j=1}^n [\exp(-\theta \|\mathbf{h}_i - \mathbf{h}_j\|_2^2) - \exp(-\theta \|\mathbf{h}'_i - \mathbf{h}'_j\|_2^2)] \right| \\
&\quad + \left| \frac{2}{mn} \sum_{i=1}^n \sum_{j=1}^m [\exp(-\theta \|\mathbf{h}_i - \mathbf{v}_j\|_2^2) - \exp(-\theta \|\mathbf{h}'_i - \mathbf{v}_j\|_2^2)] \right| \\
&\stackrel{(a)}{\leq} \frac{\sqrt{\theta}}{n^2} \sum_{i,j=1}^n |\|\mathbf{h}_i - \mathbf{h}_j\|_2 - \|\mathbf{h}'_i - \mathbf{h}'_j\|_2| + \frac{2\sqrt{\theta}}{mn} \sum_{i=1}^n \sum_{j=1}^m |\|\mathbf{h}_i - \mathbf{v}_j\|_2 - \|\mathbf{h}'_i - \mathbf{v}_j\|_2| \\
&\stackrel{(b)}{\leq} \frac{\sqrt{\theta}}{n^2} \sum_{i,j=1}^n \|(\mathbf{h}_i - \mathbf{h}'_i) - (\mathbf{h}_j - \mathbf{h}'_j)\|_2 + \frac{2\sqrt{\theta}}{mn} \sum_{i=1}^n \sum_{j=1}^m \|(\mathbf{h}_i - \mathbf{h}'_i) - (\mathbf{v}_j - \mathbf{v}_j)\|_2 \\
&\leq \frac{4\sqrt{\theta}}{n} \sum_{i=1}^n \|\mathbf{h}_i - \mathbf{h}'_i\|_2 \\
&\stackrel{(c)}{\leq} 4\sqrt{\frac{\theta}{n}} \|\mathbf{H} - \mathbf{H}'\|_F
\end{aligned}$$

In the above derivation, (a) holds due to $|\exp(-x^2) - \exp(-y^2)| \leq |x - y|$ for any $x, y \geq 0$, (b) holds due to the triangle inequality, and (c) holds by the Cauchy–Schwarz inequality.

The output of the layer is \mathbf{S} , for which we have

$$\begin{aligned}
\|\mathbf{S} - \mathbf{S}'\|_2 &= \sqrt{\sum_{i=1}^N \sum_{j=1}^R |s_{ij} - s'_{ij}|^2} \\
&\leq 4\sqrt{\frac{\theta}{n}} \sqrt{\sum_{i=1}^N \sum_{j=1}^R \|\mathbf{H}_i - \mathbf{H}'_i\|_F^2} \\
&= 4\sqrt{\frac{\theta R}{n}} \|\mathbf{H} - \mathbf{H}'\|_F
\end{aligned}$$

This finished the proof. □

Lemma E.5. Suppose the GIN f has Q layers and each layer has an MLP of Q' layers. Then the Lipschitz constant of f is $L_{GIN} = \max_{i \in [N]} \|\mathbf{A}_i\|_2^Q \prod_{j=1}^{QQ'} \|\mathbf{W}_j\|_2$.

Proof. Recall that the l -th layer of the GIN can be formulated as

$$f^{(l)}(\mathbf{A}, \mathbf{Z}^{(l-1)}) = \text{MLP}^{(l)}((\mathbf{A} + \epsilon \mathbf{I}) \cdot \mathbf{Z}^{(l-1)}) \quad (49)$$

where $\mathbf{Z}^{(0)} = \mathbf{X}$. For convenience, let $\epsilon = 0$. We put all adjacency matrices together to form a big block diagonal matrix $\bar{\mathbf{A}}$ of size $Nn \times Nn$. Then the spectral norm of $\bar{\mathbf{A}}$ is $\max_{i \in [N]} \|\mathbf{A}_i\|_2$. Similarly, we form a big matrix $\bar{\mathbf{Z}}$ of size $Nn \times d$. Then we have

$$\bar{Z}^{(l)} = f^{(l)}(\bar{\mathbf{A}}, \bar{\mathbf{Z}}^{(l-1)}) = \text{MLP}^{(l)}(\bar{\mathbf{A}} \bar{\mathbf{Z}}^{(l-1)}) \quad (50)$$

Then the Lipschitz constant of $f^{(l)}$ is $\max_{i \in [N]} \|\mathbf{A}_i\|_2 \prod_{j=1}^Q \rho_j \|\mathbf{W}_j\|_2$, where W_j is the weight matrix and ρ_j is the Lipschitz constant of the layer. Since most activation functions such as ReLu and Sigmoid are 1-Lipschitz, we let $\rho_i = 1 \forall i$. Given that f has Q layers, we conclude that the Lipschitz constant is $\max_{i \in [N]} \|\mathbf{A}_i\|_2^Q \prod_{j=1}^{QQ'} \|\mathbf{W}_j\|_2$. □

Lemma E.6. Suppose the graph transformer g is composed of Q blocks and each block has an MLP of Q' layers. Suppose the attention map is μ -Lipschitz. Then the Lipschitz constant of g is $L_{GT} = \mu^{QQ'} \prod_{j=1}^{QQ'} \|\mathbf{W}_j\|_2$.

Proof. Recall that the self-attention is

$$\text{attn}\left(\boldsymbol{\Gamma}_i^{(j)}\right) = \text{softmax}\left(\frac{(\boldsymbol{\Gamma}_i^{(j)} \mathbf{W}_Q)(\boldsymbol{\Gamma}_i^{(j)} \mathbf{W}_K)^\top}{\sqrt{d'}}\right)(\boldsymbol{\Gamma}_i^{(j)} \mathbf{W}_V) \quad (51)$$

Assume that the softmax operation is μ -Lipschitz with respect to the input $\boldsymbol{\Gamma}_i^{(j)}$. The Lipschitz constant of the self-attention mechanism is $\mu \|\mathbf{W}_V\|_2$. The self-attention is then followed by a residual connection, layer normalization, and MLP of Q -layers. We omit the residual connection and the layer normalization since they have a tiny impact on the analysis. For the MLP, the Lipschitz constant is $\prod_{j=1}^{Q'} \|\mathbf{W}_j\|_2$, where \mathbf{W}_j is the weight matrix of layer j and the activation functions are assumed to be 1-Lipschitz. Since g has Q sequential blocks, the total Lipschitz constant is $\mu^{QQ'} \prod_{j=1}^{Q'} \|\mathbf{W}_j\|_2$. \square

Lemma E.7 (Lemma 3.2 in [Bartlett et al., 2017]). *Let conjugate exponents (p, q) and (r, s) be given with $p \leq 2$, as well as positive reals (a, b, ϵ) and positive integer m . Let matrix $\mathbf{X} \in \mathbb{R}^{n \times d}$ be given with $\|\mathbf{X}\|_p \leq b$. Then*

$$\ln \mathcal{N}(\{\mathbf{X}\mathbf{A} : \mathbf{A} \in \mathbb{R}^{d \times m}, \|\mathbf{A}\|_{q,s} \leq a\}, \epsilon, \|\cdot\|_F) \leq \left\lceil \frac{a^2 b^2 m^{2/r}}{\epsilon^2} \right\rceil \ln(2dm)$$

Lemma E.8. *Suppose $\mathbf{Z}_i \in \mathbb{R}^{n \times d}$ and $f_i(\mathbf{Z}_i)$ is L_i -Lipschitz continuous with respect to \mathbf{Z}_i , where $i = 1, \dots, Q$. Let $\bar{\mathbf{Z}} = [\mathbf{Z}_1; \dots; \mathbf{Z}_Q] \in \mathbb{R}^{n \times dQ}$. Let $F = [f_1, f_2, \dots, f_Q]$. Then the Lipschitz constant of $F(\bar{\mathbf{Z}})$ with respect to $\bar{\mathbf{Z}}$ is $L_F = \max_i \alpha_i$.*

Proof. Based on the settings, we have

$$\begin{aligned} & \|F(\bar{\mathbf{Z}}) - F(\bar{\mathbf{Z}}')\|_F \\ &= \|f_1(\mathbf{Z}_1) - f_1(\mathbf{Z}'_1) \quad \dots \quad f_Q(\mathbf{Z}_Q) - f_Q(\mathbf{Z}'_Q)\|_F \\ &= \sqrt{\sum_{i=1}^Q \|f_i(\mathbf{Z}_i) - f_i(\mathbf{Z}'_i)\|_F^2} \\ &\leq \sqrt{\sum_{i=1}^Q \alpha_i^2 \|\mathbf{Z}_i - \mathbf{Z}'_i\|_F^2} \\ &\leq \max_i \alpha_i \sqrt{\sum_{i=1}^Q \|\mathbf{Z}_i - \mathbf{Z}'_i\|_F^2} \\ &= \max_i \alpha_i \|\bar{\mathbf{Z}} - \bar{\mathbf{Z}}'\|_F \end{aligned} \quad (52)$$

\square

Lemma E.9. *Suppose ϕ is an α -Lipschitz continuous function, then $\ln \mathcal{N}(\epsilon, \phi \circ \mathcal{F}, \rho) \leq \ln \mathcal{N}(\epsilon/\alpha, \mathcal{F}, \rho)$.*

Proof. This is a well-known result, and we will not repeat the proof. \square

The theorem shows the impacts of model architecture, input data size, and weight matrices on the generalization ability of our model:

- When the total number of training graphs MN is larger, the bound is tighter, which is further verified by the experiments in Figure 2. Note that if we use the unsupervised contrastive loss to train the model, due to the data augmentation (though the samples are not independent), the generalization could be stronger.
- Although β often scales with \sqrt{n} , we have a factor $\frac{1}{\sqrt{n}}$ in L_F . This means that the number of nodes in each graph does not have a significant impact on the generalization, provided that the spectral norms of $\mathbf{A}_i^{(j)}$ increase slowly with n . As a result, our model will generalize well to both small graphs (e.g., ENZYMES) and large graphs (e.g., REDDIT), as shown by Tables 1 and 3.
- Since L_F scales with $\mathcal{O}(\sqrt{\gamma R})$, we could use a relatively large R to enrich the final vector representation for each graph, thereby improving the expressiveness. Moreover, L_F is not very sensitive to γ , which is learned adaptively.

Table 6: Dataset Statistics.

Dataset	Domain	#Graphs	#Avg. Nodes	#Features	#Classes	Task
ENZYMEs	Bioinformatics	600	32.63	21	6	Graph Classification/Graph Clustering
NCI1	Small molecules	4110	29.87	37	2	Graph Classification/Graph Clustering
NCI109	Small molecules	4127	29.68	38	2	Graph Classification
DD	Bioinformatics	1178	284.32	89	2	Graph Classification
Mutagenicity	Small molecules	4337	30.32	14	2	Graph Classification
COLLAB	Social networks	5000	74.49	0	2	Graph Classification/Graph Clustering
REDDIT-BINARY	Social networks	2000	429.63	0	2	Graph Classification/Graph Clustering
REDDIT-MULTI	Social networks	4999	508.52	0	5	Graph Clustering
IMDB-BINARY	Social networks	1000	19.77	0	2	Graph Classification
IMDB-MULTI	Social networks	1500	13.00	0	3	Graph Classification
Letter-med	Computer vision	2250	4.67	2	15	Graph Classification
COIL-RAG	Computer vision	3900	3.01	64	100	Graph Classification
Cuneiform	Computer vision	267	21.27	10	30	Graph Classification

F GIN and Graph Transformer based Model

To design a universal graph representation model F , we incorporate two main components: a GNN module f and a graph transformer module g . We build GNN encoder on top of transformer encoder $g_\psi \circ f_\theta(\cdot)$. The GNN encoder specializes in learning local representations of the structure of a node’s immediate neighborhood, while the transformer computes all pairwise node interactions, enabling global reasoning through attention mechanisms. Specifically, we adopt the Graph Isomorphism Network (GIN) [Xu et al., 2019] as the GNN encoder, and its l -th layer can be formulated as

$$f^{(l)} \left(\mathbf{A}_i^{(j)}, \mathbf{Z}_i^{(j)} \right) = \text{MLP}^{(l)} \left(\left(\tilde{\mathbf{A}}_i^{(j)} + \epsilon \mathbf{I} \right) \cdot \mathbf{Z}_i^{(j)} \right) \quad (53)$$

where $\tilde{\mathbf{A}}_i^{(j)}$ is the adjacency matrix of $G_i^{(j)}$ with self-loops, ϵ is a hyperparameter, $\text{MLP}^{(l)}$ is a multilayer perceptron (MLP) in layer l , and the parameters to optimize are denoted as θ .

The graph transformer (GT) module consists of a self-attention mechanism and a feed-forward network, which is usually an MLP. Let $\mathbf{\Gamma}_i^{(j)} \in \mathbb{R}^{n_i \times d}$ represent the matrix of hidden states, and \mathbf{W}_Q , \mathbf{W}_K , and \mathbf{W}_V of size $d \times d'$ be projection matrices, the self-attention mechanism is

$$\text{attn} \left(\mathbf{\Gamma}_i^{(j)} \right) = \text{softmax} \left(\frac{(\mathbf{\Gamma}_i^{(j)} \mathbf{W}_Q)(\mathbf{\Gamma}_i^{(j)} \mathbf{W}_K)^\top}{\sqrt{d'}} \right) (\mathbf{\Gamma}_i^{(j)} \mathbf{W}_V) \quad (54)$$

which is further transformed to $\hat{\mathbf{\Gamma}}_i^{(j)} = \text{Norm} \left(\mathbf{\Gamma}_i^{(j)} + \text{attn} \left(\mathbf{\Gamma}_i^{(j)} \right) \right)$. Then the l -th transformer block can be formulated as

$$g^{(l)} \left(\mathbf{\Gamma}_i^{(j)} \right) = \text{Norm} \left(\hat{\mathbf{\Gamma}}_i^{(j)} + \text{FFN} \left(\hat{\mathbf{\Gamma}}_i^{(j)} \right) \right) \quad (55)$$

We denote the parameters of the transformer module as ψ . Finally, we concatenate the outputs of the GIN and GT, leading to the following node representations of $G_i^{(j)}$:

$$\mathbf{H}_i^{(j)} = g_\psi \circ f_\theta \left(\mathbf{A}_i^{(j)}, \mathbf{Z}_i^{(j)} \right) \parallel f_\theta \left(\mathbf{A}_i^{(j)}, \mathbf{Z}_i^{(j)} \right), \quad i \in [N_j], \quad j \in [M]. \quad (56)$$

For convenience, we let $\mathcal{W} = \{\psi, \theta\}$, which is the set of all parameters of the GIN and GT.

G Details about Experimental Settings

G.1 Datasets

The basic information and statistics of the graph datasets we used in the experiments are shown in Table 6. In our experiments, the concatenation of the original node attributes and node labels in the datasets is used as initial input node features.

G.2 Details of Model Testing in Few-Shot Graph Classification

Specifically, let the dataset in the downstream task be $\mathcal{G}^{\text{Down}} = \{\mathcal{G}^{\text{train}}, \mathcal{G}^{\text{test}}\}$, where $\mathcal{G}^{\text{train}} = \{(\mathbf{A}_i^{\text{train}}, \mathbf{X}_i^{\text{train}})\}_{i=1}^{N_{\text{train}}}$ and $\mathcal{G}^{\text{test}} = \{(\mathbf{A}_i^{\text{test}}, \mathbf{X}_i^{\text{test}})\}_{i=1}^{N_{\text{test}}}$. For $\mathcal{G}^{\text{train}}$, applying (2), (3), (4), and (5) sequentially, we obtain $\mathbf{Z}^{\text{train}}$, the aligned node

feature matrix of the training set, which is further modified by using Algorithm 1. Now we apply the pretrained model to $\mathbf{Z}^{\text{train}}$ to obtain the embedding vector of each training graph, i.e., $\mathbf{g}_i^{\text{train}} = F_{\mathcal{W}, \mathcal{V}, \gamma}(\mathbf{A}_i^{\text{train}}, \mathbf{Z}_i^{\text{train}})$, $i \in N_{\text{train}}$.

Let the kernel matrix of the training set be $\mathbf{K}_{\lambda_q}^{\text{train}} = \mathbf{U} \boldsymbol{\Sigma} \mathbf{V}^{\top}$, and the cross-kernel matrix between the test and training sets be $\mathbf{K}_{\lambda_q}^{\text{test}}$. $\mathbf{Z}_{\lambda_q}^{\text{test}} = \mathbf{K}_{\lambda_q}^{\text{test}} \mathbf{V}_{\bar{d}} \boldsymbol{\Sigma}_{\bar{d}}^{-1/2}$, $q \in [Q]$. Then we obtain $\mathbf{Z}^{\text{test}} = [\mathbf{Z}_{\lambda_1}^{\text{test}}, \mathbf{Z}_{\lambda_2}^{\text{test}}, \dots, \mathbf{Z}_{\lambda_Q}^{\text{test}}]$, the aligned node feature matrix of the testing set, which is further modified by using Algorithm 1. Now, similar to the training data, we have $\mathbf{g}_i^{\text{test}} = F_{\mathcal{W}, \mathcal{V}, \gamma}(\mathbf{A}_i^{\text{test}}, \mathbf{Z}_i^{\text{test}})$, $i \in N_{\text{test}}$. These steps are summarized in Algorithm 3, where the underlined values are frozen in Algorithm 1.

Algorithm 3 Few-shot graph classification

Input: $\mathcal{G}^{\text{Down}} = \{\mathcal{G}^{\text{train}}, \mathcal{G}^{\text{test}}\}$, $\{\mathbf{R}_{\text{pre}}^{(j)}\}_{j=1}^M$, $\{\boldsymbol{\mu}_{\text{pre}}^{(j)}\}_{j=1}^M$
 1: Compute $\mathbf{Z}^{\text{train}}$, \mathbf{Z}^{test} using (4) and (5).
 2: $\mathbf{R}^{\text{train}} \leftarrow \text{Algorithm 1}(\boldsymbol{\mu}^{\text{train}}, \{\boldsymbol{\mu}_{\text{pre}}^{(j)}\}_{j=1}^M, \{\mathbf{R}_{\text{pre}}^{(j)}\}_{j=1}^M)$
 $\mathbf{R}^{\text{test}} \leftarrow \text{Algorithm 1}(\boldsymbol{\mu}^{\text{test}}, \boldsymbol{\mu}^{\text{train}}, \mathbf{R}^{\text{train}}, \{\boldsymbol{\mu}_{\text{pre}}^{(j)}\}_{j=1}^M, \{\mathbf{R}_{\text{pre}}^{(j)}\}_{j=1}^M)$
 3: Mean alignment: $\mathbf{Z}^{\text{train}} \leftarrow \mathbf{Z}^{\text{train}} \mathbf{R}^{\text{train}}^{\top}$, $\mathbf{Z}^{\text{test}} \leftarrow \mathbf{Z}^{\text{test}} \mathbf{R}^{\text{test}}^{\top}$.
 4: Representation: $\mathbf{g}_i^{\text{train}} \leftarrow F_{\mathcal{W}, \mathcal{V}, \gamma}(\mathbf{A}_i^{\text{train}}, \mathbf{Z}_i^{\text{train}})$, $i \in [\mathcal{G}^{\text{train}}]$
 5: Train the softmax classifier f_c on $\{\mathbf{g}_i^{\text{train}}\}$.
 6: $\hat{\mathbf{y}}_i^{\text{test}} = f_c \circ F_{\mathcal{W}, \mathcal{V}, \gamma}(\mathbf{A}_i^{\text{test}}, \mathbf{Z}_i^{\text{test}})$, $i \in [\mathcal{G}^{\text{test}}]$.
Output: Predicted graph labels $\{\hat{\mathbf{y}}_i^{\text{test}}\}$

G.3 Implementation Details

In our experiments, we use 6 Gaussian kernels with different $\lambda_q \in \{0.25, 0.5, 1, 2, 5, 10\}$. For all kernel matrices and the adjacency matrix, the truncated dimension of SVD \bar{d} is set as 32. For each global graph obtained by Gaussian kernels, we use 6-GIN encoder to encode node features from different global graphs respectively. We implement each GIN encoder with 3 graph convolutional layers. The size of each hidden layer in GIN is set to 128. The graph transformer module consists of 3 equally wide layers, each containing 4 attention heads, with the dimension of each attention head set as 48. In the pre-training stage, all modules are optimized using Adam optimizer [Kinga et al., 2015] with fixed learning rate $\alpha_1 = 0.0005$ and a weight decay factor of 10^{-5} , trained for 50 epochs. The Gaussian kernel parameter γ in the reference layer employs a separate learning rate $\alpha_2 = 0.1$. The batch size for all datasets is fixed to 64.

Few-shot learning settings In the downstream tasks of few-shot graph classification, the classifier is a softmax classifier, which follows the setting in EdgePrompt [Fu et al., 2025]. Regarding data splitting, we randomly choose 50 graphs in each class for training, and the remaining samples are used for testing. The number of epochs is set to 500, and the learning rate of the classifier is set to 0.001 for graph few-shot training. As the k-shot tasks are balanced classification, we employ accuracy as the evaluation metric following EdgePrompt.

For ProNoG, we used the provided checkpoint from the official open-source repository as the pretrained model. For BRIDGE, GFT, and RiemannGFM, we followed the recommended settings in their paper to pretrain the model. The official repository of RiemannGFM does not support graph classification, we extend it to graph level task by using mean pooling. In the downstream adaptation stage, we adopted the recommended hyperparameters for both methods. Experiments on COLLAB, REDDIT-B, IMDB-B, IMDB-M, and Letter-med are conducted under 50-shot setting following experiments in our paper. For COIL-RAG and Cuneiform, due to a lack of enough samples per class, we adopt 5-shot and 1-shot settings, respectively. Since the three baselines do not handle datasets without node attributes, to ensure fair comparison, we handle social network datasets without node attributes (COLLAB, REDDIT-B, IMDB-B, IMDB-M) uniformly across all methods. Following our proposed approach, we generate node attributes using truncated SVD on $\mathbf{A} + \mathbf{I}$ (adjacency matrix with self-loops) as input for all baseline models. All the results of our method are obtained from models trained on 5 bio-chemical datasets (ENZYMEs, DD, NCI1, NCI109, Mutagenicity) mentioned in the main part of the paper, which differ significantly from social networks and computer vision data in both semantics and structure.

Unsupervised pre-training settings Following You et al. [2020], we construct 3 augmentations using dropping nodes with a ratio of 0.1, permuting edges with a ratio of 0.1, and extracting subgraph for each graph before the global multi-graph construction and max-density mean alignment.

We conduct all experiments on a 14 vCPU Intel(R) Xeon(R) Gold 6348 CPU with one Nvidia A800-80G GPU, CUDA 11.8. We repeat five times with different random seeds and report the average results with standard deviation calculated by the numpy library function.

H More Results

H.1 Intuitive Example of the Global Graph Construction

Here we provide an intuitive example of synthetic data to show that our graph construction could be domain-agnostic. Suppose we have four datasets $\mathcal{D}_1, \mathcal{D}_2, \mathcal{D}_3, \mathcal{D}_4$ drawn from the following four distributions respectively: 1) $\mathcal{N}(\mathbf{0}, \mathbf{I}_2)$ (2D Gaussian); 2) $\mathcal{N}(\mathbf{0}, \mathbf{I}_2)$ (2D Gaussian); 3) $\mathcal{N}(\mathbf{1}, 2\mathbf{I}_3)$ (3D Gaussian); 4) $\mathcal{N}(-\mathbf{2}, \mathbf{I}_2) + \mathcal{N}(\mathbf{2}, \mathbf{I}_2)$ (2D Gaussian mixture model). Thus, \mathcal{D}_2 can be regarded as a dataset from the same domain as \mathcal{D}_1 , while \mathcal{D}_3 and \mathcal{D}_4 are from different domains. We calculate the Gromov-Wasserstein distances between the weighted graphs constructed from the four datasets using the method proposed in our paper. The results are shown in the following table (average of 5 runs). We see that the distance between \mathcal{D}_1 and \mathcal{D}_3 is close to that between \mathcal{D}_1 and \mathcal{D}_2 , meaning that the features generated by our multi-graph alignment method are indeed domain agnostic. The distance between \mathcal{D}_1 and \mathcal{D}_4 is much larger than that between \mathcal{D}_1 and \mathcal{D}_3 , meaning that our method can effectively identify the topological difference between the datasets.

Table 7: Gromov-Wasserstein distances between synthetic datasets (average of 5 runs)

	$\mathcal{D}_1 \sim \mathcal{N}(\mathbf{0}, \mathbf{I}_2)$	$\mathcal{D}_2 \sim \mathcal{N}(\mathbf{0}, \mathbf{I}_2)$	$\mathcal{D}_3 \sim \mathcal{N}(\mathbf{1}, 2\mathbf{I}_3)$	$\mathcal{D}_4 \sim \mathcal{N}(-\mathbf{2}, \mathbf{I}_2) + \mathcal{N}(\mathbf{2}, \mathbf{I}_2)$
$\mathcal{D}_1 \sim \mathcal{N}(\mathbf{0}, \mathbf{I}_2)$	0	0.004	0.015	0.069
$\mathcal{D}_2 \sim \mathcal{N}(\mathbf{0}, \mathbf{I}_2)$	—	0	0.015	0.069
$\mathcal{D}_3 \sim \mathcal{N}(\mathbf{1}, 2\mathbf{I}_3)$	—	—	0	0.081
$\mathcal{D}_4 \sim \mathcal{N}(-\mathbf{2}, \mathbf{I}_2) + \mathcal{N}(\mathbf{2}, \mathbf{I}_2)$	—	—	—	0

H.2 Full Results of Table 1

The full compared numbers in the baseline of Table 1 are provided in Table 8.

H.3 Extension to Node Classification Task

Our model can also be extended to node-level tasks by retraining it with a node-level contrastive loss objective. Specifically, we maintain the construction of global multi-graphs and the mean alignment module from our original framework, while removing the reference distribution layers since graph-level representations are not required here. The node embeddings are obtained directly from the outputs of both the Graph Transformer and GIN modules. These embeddings are then fed into a linear classifier to perform the downstream node classification task.

The model was evaluated on 4 node classification datasets: Cora, citepSeer, PubMed, and ogbn-arxiv. The 5-shot node classification results are shown in Table 9. This adaptation demonstrates that GraphVec-FM can also be effectively extended to node-level tasks.

H.4 The Impact of Nyström Approximation

To address the computational complexity associated with large-scale graphs, we employ the Nyström approximation during pre-training. To systematically evaluate its impact, we pre-train GraphVec-FM using the Nyström method with varying sample sizes, while keeping the pre-training datasets consistent with our main experiments. In Table ??, we specifically report the wall-clock time required for constructing the global multi-graphs, and evaluate downstream performance via 50-shot graph classification accuracy on the Letter-med dataset. We see that, when the sample size is less than 2000, the time used for constructing global multi-graphs is acceptable. When adding the sample size to 4000, the wall-clock time increases sharply while the performance improvement is marginal (less than 0.1%).

H.5 Impact of Number of Pre-training Datasets

Figure 2 shows the change of classification accuracy when the number of datasets used in pre-training increases from 1 to 4. We can see that with more datasets used in pre-training, the performance in downstream tasks becomes better. This result indicates that the generalization ability of graph embeddings generated by our GraphVec-FM can benefit

Table 8: 50-shot graph classification performance comparison with different pre-trained models. We color the **best** and **second best** models. The compared numbers of in-domain experiments are from EdgePrompt [Fu et al., 2025].

Pre-training	Tuning Methods	ENZYMES	DD	NCI1	NCI109	Mutagenicity	Average
GraphCL	Classifier Only	30.50 \pm 1.16	62.89 \pm 2.19	62.49 \pm 1.95	61.68 \pm 0.93	66.62 \pm 1.87	56.84
	GraphPrompt [Liu et al., 2023b]	27.83 \pm 1.61	64.33 \pm 1.79	63.19 \pm 1.71	62.18 \pm 0.48	67.62 \pm 0.65	57.03
	ALL-in-one [Sun et al., 2023b]	25.92 \pm 0.55	66.54 \pm 1.82	57.52 \pm 2.61	62.74 \pm 0.78	63.43 \pm 2.53	55.23
	GPF [Fang et al., 2023]	30.08 \pm 1.25	64.54 \pm 2.22	62.66 \pm 1.83	62.29 \pm 0.90	66.54 \pm 1.85	57.22
	GPF-plus [Fang et al., 2023]	31.00 \pm 1.50	67.26 \pm 2.29	64.56 \pm 1.10	62.84 \pm 0.22	66.82 \pm 1.63	58.50
	EdgePrompt [Fu et al., 2025]	29.50 \pm 1.57	64.16 \pm 2.13	63.05 \pm 2.11	62.59 \pm 0.93	66.87 \pm 1.88	57.23
	EdgePrompt+ [Fu et al., 2025]	34.00 \pm 1.25	67.98 \pm 2.05	66.30 \pm 2.54	66.52 \pm 0.91	67.47 \pm 2.37	60.45
SimGRACE	Classifier Only	27.07 \pm 1.04	61.77 \pm 2.40	61.27 \pm 3.64	62.12 \pm 1.10	67.36 \pm 0.71	55.92
	GraphPrompt [Liu et al., 2023b]	26.87 \pm 1.47	62.58 \pm 1.84	62.45 \pm 1.52	62.41 \pm 0.69	68.03 \pm 0.78	56.47
	ALL-in-one [Sun et al., 2023b]	25.73 \pm 1.18	65.16 \pm 1.47	58.52 \pm 1.59	62.01 \pm 0.66	64.43 \pm 1.00	55.17
	GPF [Fang et al., 2023]	28.53 \pm 1.76	65.64 \pm 0.70	61.45 \pm 3.13	61.90 \pm 1.26	67.19 \pm 0.74	56.94
	GPF-plus [Fang et al., 2023]	27.33 \pm 2.01	67.20 \pm 1.56	61.61 \pm 2.89	62.84 \pm 0.23	67.69 \pm 0.64	57.33
	EdgePrompt [Fu et al., 2025]	29.33 \pm 2.30	63.97 \pm 2.14	62.02 \pm 3.02	62.02 \pm 1.03	67.55 \pm 0.85	56.98
	EdgePrompt+ [Fu et al., 2025]	32.67 \pm 2.53	67.72 \pm 1.62	67.07 \pm 1.96	66.53 \pm 1.30	68.31 \pm 1.36	60.46
EP-GPPT	Classifier Only	29.08 \pm 1.35	62.12 \pm 2.82	56.85 \pm 4.35	62.27 \pm 0.78	66.30 \pm 1.78	55.32
	GraphPrompt [Liu et al., 2023b]	26.67 \pm 1.60	61.61 \pm 1.91	58.77 \pm 0.97	62.16 \pm 0.89	66.37 \pm 1.17	55.12
	ALL-in-one [Sun et al., 2023b]	24.92 \pm 1.33	63.61 \pm 2.12	59.14 \pm 2.12	59.70 \pm 1.37	64.86 \pm 1.60	54.45
	GPF [Fang et al., 2023]	28.33 \pm 1.73	63.48 \pm 2.08	58.14 \pm 4.16	62.52 \pm 1.39	66.10 \pm 0.96	55.71
	GPF-plus [Fang et al., 2023]	29.25 \pm 1.30	66.92 \pm 2.34	62.93 \pm 3.23	64.13 \pm 1.42	67.57 \pm 1.45	58.16
	EdgePrompt [Fu et al., 2025]	28.33 \pm 3.41	64.03 \pm 2.26	59.85 \pm 3.15	62.98 \pm 1.44	66.36 \pm 1.22	56.31
	EdgePrompt+ [Fu et al., 2025]	32.75 \pm 2.26	66.16 \pm 1.60	63.58 \pm 2.07	65.15 \pm 1.60	68.35 \pm 1.57	59.20
EP-GraphPrompt	Classifier Only	31.33 \pm 3.22	62.58 \pm 2.40	62.09 \pm 2.31	60.19 \pm 1.71	65.13 \pm 0.81	55.32
	GraphPrompt [Liu et al., 2023b]	30.20 \pm 1.93	64.72 \pm 1.98	62.57 \pm 1.45	62.32 \pm 0.95	65.85 \pm 0.65	57.13
	ALL-in-one [Sun et al., 2023b]	29.07 \pm 1.16	65.60 \pm 2.38	58.67 \pm 2.42	57.69 \pm 1.08	64.66 \pm 0.76	55.14
	GPF [Fang et al., 2023]	30.93 \pm 1.76	66.21 \pm 1.66	61.80 \pm 2.78	62.27 \pm 1.18	65.61 \pm 0.59	57.36
	GPF-plus [Fang et al., 2023]	30.67 \pm 3.06	67.50 \pm 2.45	62.59 \pm 2.09	61.98 \pm 1.60	65.51 \pm 1.10	57.65
	EdgePrompt [Fu et al., 2025]	30.80 \pm 2.09	65.87 \pm 1.35	61.75 \pm 2.49	62.33 \pm 1.65	65.77 \pm 0.90	57.30
	EdgePrompt+ [Fu et al., 2025]	33.27 \pm 2.71	67.47 \pm 2.14	65.06 \pm 1.84	64.64 \pm 1.57	66.42 \pm 1.31	59.37
cross-domain	GCN [Kipf and Welling, 2017]	43.33 \pm 1.05	65.84 \pm 2.77	61.36 \pm 2.00	62.17 \pm 0.66	60.46 \pm 1.75	58.63
	BRIDGE [Yuan et al., 2025a]	36.67 \pm 5.96	64.95 \pm 3.38	63.50 \pm 2.27	61.78 \pm 1.63	65.12 \pm 2.83	58.40
	GFT [Wang et al., 2024b]	34.61 \pm 3.12	56.00 \pm 1.77	59.16 \pm 6.25	60.50 \pm 2.71	67.82 \pm 3.18	55.61
	RiemannGFM [Sun et al., 2025]	34.27 \pm 1.72	68.74 \pm 1.31	55.10 \pm 2.24	59.86 \pm 1.30	62.56 \pm 4.04	56.11
Unsupervised GraphVec-FM	GraphVec-FM	51.00 \pm 3.22	75.94 \pm 2.70	67.32 \pm 1.51	67.90 \pm 1.67	68.57 \pm 1.62	66.14
	Unsupervised GraphVec-FM	48.33 \pm 2.36	74.02 \pm 1.26	66.11 \pm 2.30	64.34 \pm 2.38	68.38 \pm 2.88	64.23
	GraphVec-FM w/o mean alignment	49.33 \pm 1.48	73.14 \pm 1.16	65.80 \pm 1.40	65.21 \pm 2.05	67.00 \pm 1.31	64.09

Table 9: 5-shot node classification results on node-level tasks

Methods	Cora	citeSeer	Pubmed	ogbn-arxiv
GPPT [Sun et al., 2022]	41.28 \pm 6.24	35.32 \pm 1.27	53.41 \pm 3.99	17.73 \pm 1.66
GraphPrompt [Liu et al., 2023b]	31.65 \pm 3.33	26.98 \pm 1.24	44.18 \pm 5.57	16.11 \pm 1.42
ALL-in-one [Sun et al., 2023b]	31.57 \pm 2.86	29.76 \pm 1.53	46.89 \pm 5.35	17.89 \pm 1.21
GPF [Fang et al., 2023]	37.56 \pm 3.81	29.74 \pm 1.73	48.16 \pm 3.32	17.64 \pm 1.18
GPF-plus [Fang et al., 2023]	28.87 \pm 3.18	26.65 \pm 1.91	43.02 \pm 4.59	17.39 \pm 1.27
EdgePrompt [Fu et al., 2025]	37.26 \pm 4.53	29.83 \pm 1.01	45.49 \pm 3.27	17.82 \pm 1.59
EdgePrompt + [Fu et al., 2025]	56.41 \pm 3.62	43.49 \pm 2.62	61.51 \pm 4.91	17.78 \pm 2.12
GraphVec-FM	58.66 \pm 1.51	45.45 \pm 1.26	65.72 \pm 2.43	23.75 \pm 1.39

Table 10: Wall-clock time and classification accuracy under different numbers of Nyström samples.

	# Nyström samples			
	100	1,000	2,000	4,000
Wall-clock Time (s)	34.82	48.57	63.55	716.61
Accuracy (%)	81.50 \pm 2.21	82.47 \pm 0.92	84.27 \pm 1.10	84.33 \pm 1.60

from the increase in the number of training datasets, which is an important capability for GFM. It can also be observed that even using model pre-trained on only 1 dataset, GraphVec-FM still outperforms other baselines shown in Table 1.

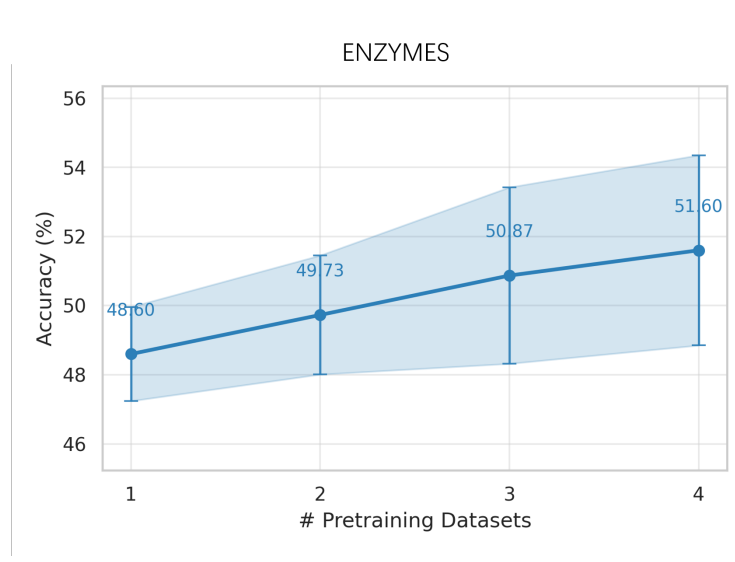


Figure 2: The change of classification accuracy in ENZYMEs when the number of datasets used in pre-training increases from 1 to 4.

H.6 Few-shot Learning with Fewer Labeled Samples

As shown in Figure 3, the classification accuracy of our method GraphVec-FM increases as the number of labeled samples increases. Our GraphVec-FM with 20-shot even outperforms the competitors with 50-shot in Table 1 of the main paper.

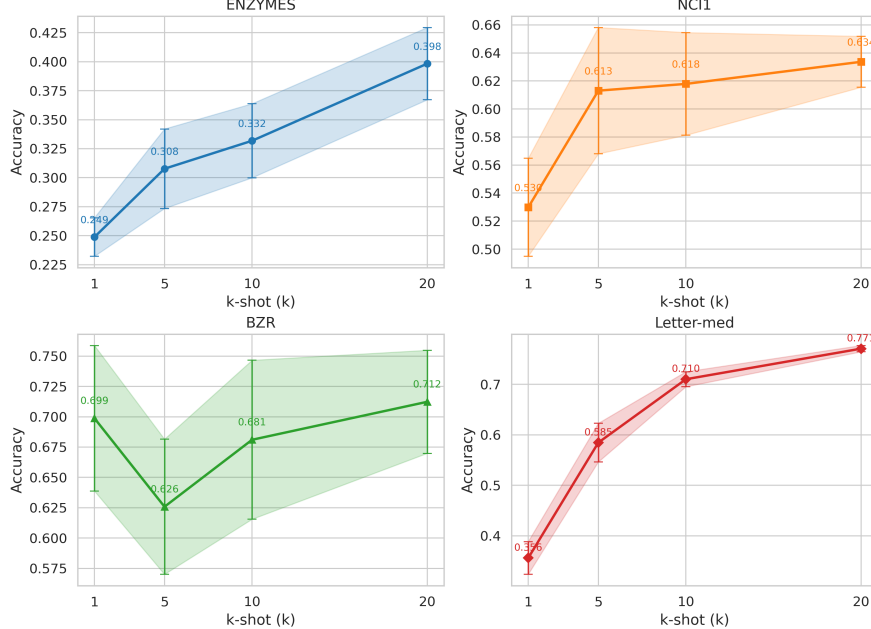


Figure 3: Classification accuracy trends of our method GraphVec-FM with varying k values in few-shot learning across four datasets (PROTEINS, NCI109, DD, and Mutagenicity), shaded area represents standard deviation

H.7 Evaluation on Generated Node Attributes SVD(A + I)

For the dataset without original node attributes, the classification mainly relies on discriminating between different structures of graphs. While the topologically derived features may not carry explicit domain semantics like chemical properties or pixel coordinates, they can be viewed as a form of generic node attribute derived from the graph connectivity. The core of our methodology, specifically the global multi-graph, is designed to bridge the inherent semantic gaps between different domains, regardless of whether the original features are rich in semantics or purely structural.

To evaluate the impact of this feature generation method and address your suggestion, we conducted a controlled experiment to replace truncated SVD with two kinds of node centrality. The results are shown in the Table 11.

Table 11: Evaluation on Generated Node Attributes.

	Degree Centrality	Betweenness Centrality	Degree + Betweenness	Our Method
REDDIT - B	73.95 ± 2.30	74.92 ± 1.68	77.79 ± 2.76	81.52 ± 1.50

As shown in the table, our method demonstrates a clear advantage over using only a single type of centrality, and also achieves a marginal improvement compared to combining both centrality measures. It is worth noting that the attributes generated by our approach can be viewed as a form of structural encoding. While other types of structural encodings may also be effective, the performance gain observed here can be largely attributed to our proposed global multi-graph construction, which enhances the model's ability to capture feature information from different spaces.

H.8 More Graph Clustering Results

To further evaluate the performance of GraphVec-FM in graph clustering task, we conduct experiments on 4 more datasets. The results are shown in Table 12. We also provide the full version of Table 2 with NMI in Table 13

Table 12: Graph clustering results on PTC-MM, MUTAG, COX2 and BZR

Dataset	PTC-MM			MUTAG			COX2			BZR		
	ACC	NMI	ARI	ACC	NMI	ARI	ACC	NMI	ARI	ACC	NMI	ARI
GraphCL+SC	62.09 ± 0.56	2.14 ± 0.43	3.36 ± 0.87	73.22 ± 2.66	32.19 ± 2.05	23.44 ± 2.45	75.01 ± 2.12	1.24 ± 0.37	2.39 ± 2.28	72.88 ± 1.66	1.90 ± 0.38	3.47 ± 0.59
GW-F [Xu et al., 2022]+SC	53.02 ± 1.66	0.36 ± 0.28	0.21 ± 0.09	73.92 ± 4.30	18.35 ± 3.85	24.48 ± 4.69	58.83 ± 4.46	1.16 ± 0.41	1.45 ± 2.21	52.76 ± 0.80	3.47 ± 1.16	-0.71 ± 0.32
GLCC [Ju et al., 2023]	61.61 ± 0.24	0.63 ± 0.41	1.24 ± 1.38	71.99 ± 3.08	13.18 ± 6.93	16.89 ± 8.28	77.37 ± 1.11	0.02 ± 0.03	-0.30 ± 0.42	63.62 ± 9.79	1.18 ± 0.60	1.12 ± 0.97
Our Method	65.74 ± 0.00	4.35 ± 0.00	6.31 ± 0.00	81.38 ± 0.00	31.00 ± 0.00	38.96 ± 0.00	78.58 ± 0.00	2.37 ± 0.00	2.19 ± 0.00	77.28 ± 0.00	0.16 ± 0.00	1.50 ± 0.00

Table 13: Graph clustering performance on ENZYMEs, NCI1, COLLAB, REDDIT-BINARY, REDDIT-MULTI. The comparison numbers are from AMGC [Yang et al., 2025].

Method	ENZYMEs			NCI1			COLLAB			REDDIT-BINARY			REDDIT-MULTI		
	ACC	NMI	ARI	ACC	NMI	ARI	ACC	NMI	ARI	ACC	NMI	ARI	ACC	NMI	ARI
RW +SC	17.0 ± 0.0	0.7 ± 0.0	0.3 ± 0.0	N/A	N/A	N/A	N/A	N/A	N/A	N/A	N/A	N/A	N/A	N/A	N/A
WL +SC	21.0 ± 0.0	3.1 ± 0.0	1.5 ± 0.0	50.1 ± 0.0	0.0 ± 0.0	0.0 ± 0.0	53.2 ± 0.0	2.0 ± 0.0	0.5 ± 0.0	57.6 ± 0.0	9.0 ± 0.0	2.2 ± 0.0	18.7 ± 0.0	9.0 ± 0.0	4.0 ± 0.0
WL-OA +SC	20.0 ± 0.0	1.4 ± 0.0	0.3 ± 0.0	53.2 ± 0.0	0.9 ± 0.0	0.8 ± 0.0	54.2 ± 0.0	0.2 ± 0.0	2.6 ± 0.0	53.8 ± 0.0	5.6 ± 0.0	3.8 ± 0.0	20.9 ± 0.0	9.6 ± 0.0	3.2 ± 0.0
SP +SC	22.0 ± 0.0	2.6 ± 0.0	1.7 ± 0.0	50.1 ± 0.0	0.1 ± 0.0	0.0 ± 0.0	48.7 ± 0.0	17.9 ± 0.0	13.9 ± 0.0	57.8 ± 0.0	2.2 ± 0.0	2.2 ± 0.0	20.3 ± 0.0	6.1 ± 0.0	0.1 ± 0.0
LT +SC	17.0 ± 0.0	0.4 ± 0.0	0.0 ± 0.0	N/A	N/A	N/A	N/A	N/A	N/A	N/A	N/A	N/A	N/A	N/A	N/A
GK +SC	17.1 ± 0.1	0.8 ± 0.3	0.0 ± 0.0	52.9 ± 0.9	0.7 ± 1.4	0.3 ± 0.6	56.8 ± 1.4	15.5 ± 1.9	9.3 ± 2.1	50.3 ± 0.3	0.2 ± 0.1	0.0 ± 0.0	18.7 ± 0.9	7.2 ± 0.3	0.3 ± 0.1
InfoGraph +KM	22.1 ± 1.0	2.4 ± 0.5	1.3 ± 0.5	54.1 ± 2.2	1.3 ± 1.1	0.9 ± 0.9	59.6 ± 1.8	14.4 ± 3.0	6.6 ± 2.3	51.3 ± 2.1	2.3 ± 4.4	0.6 ± 0.2	20.3 ± 0.9	0.5 ± 0.2	0.0 ± 0.0
InfoGraph +SC	23.8 ± 0.5	4.6 ± 0.7	2.2 ± 0.4	54.9 ± 1.7	0.9 ± 0.6	1.0 ± 0.8	60.9 ± 2.5	15.4 ± 3.3	9.3 ± 3.5	50.8 ± 1.3	1.6 ± 0.6	0.6 ± 0.0	24.7 ± 1.3	4.8 ± 0.6	3.2 ± 0.6
GraphCL +KM	21.5 ± 0.2	1.6 ± 0.1	0.9 ± 0.1	55.4 ± 1.7	0.5 ± 0.3	1.0 ± 0.9	58.0 ± 1.2	17.8 ± 2.0	11.3 ± 0.6	51.9 ± 3.3	3.4 ± 1.2	0.2 ± 0.0	25.3 ± 0.9	5.3 ± 0.3	4.3 ± 0.6
GraphCL +SC	25.3 ± 0.3	4.8 ± 0.4	2.0 ± 0.3	50.8 ± 1.6	0.6 ± 0.6	1.1 ± 0.8	57.8 ± 0.6	17.0 ± 1.3	10.1 ± 0.7	55.9 ± 2.1	3.2 ± 1.0	0.3 ± 0.2	27.3 ± 1.3	5.4 ± 0.8	4.2 ± 1.1
JOAO + KM	21.7 ± 0.4	4.9 ± 0.4	2.1 ± 0.2	51.1 ± 0.4	0.4 ± 0.2	0.1 ± 0.0	58.3 ± 1.5	18.7 ± 2.6	11.1 ± 1.8	54.3 ± 2.9	4.2 ± 1.8	0.8 ± 0.3	26.6 ± 0.6	3.6 ± 1.2	2.9 ± 0.2
JOAO + SC	24.4 ± 1.4	3.2 ± 0.7	1.7 ± 0.8	51.5 ± 3.0	0.9 ± 1.2	0.4 ± 1.2	58.2 ± 0.9	17.1 ± 2.1	10.6 ± 0.8	55.9 ± 1.2	6.7 ± 2.0	1.4 ± 0.6	25.6 ± 0.6	2.5 ± 0.2	3.4 ± 0.3
GLCC	24.4 ± 1.4	3.2 ± 0.7	1.7 ± 0.8	60.9 ± 2.3	5.3 ± 1.9	3.6 ± 2.6	60.3 ± 0.6	18.2 ± 1.3	12.1 ± 0.9	67.6 ± 3.4	9.2 ± 2.6	8.7 ± 1.7	32.4 ± 2.1	11.8 ± 1.3	8.2 ± 1.6
AMGC	26.7 ± 2.0	5.2 ± 1.3	2.8 ± 0.7	62.7 ± 3.0	6.4 ± 1.9	6.4 ± 3.6	61.2 ± 1.0	20.5 ± 1.6	12.9 ± 0.9	64.3 ± 1.9	12.1 ± 3.3	10.5 ± 2.7	35.5 ± 2.3	16.1 ± 0.9	12.0 ± 0.7
GraphVec-FM	29.1 ± 0.4	7.7 ± 0.3	3.5 ± 0.2	64.8 ± 0.0	6.5 ± 0.0	8.7 ± 0.0	61.8 ± 0.0	21.2 ± 0.0	18.9 ± 0.0	71.6 ± 0.0	20.7 ± 0.0	18.6 ± 0.0	40.0 ± 0.2	17.3 ± 0.1	12.1 ± 0.2

H.9 Visualization of aligned node embeddings

We visualize the node embeddings from different domains after the global multi-graph construction and mean alignment using T-SNE. As shown in Figure 4, the distance between node embeddings from different domains is even larger than that from the same domain. This observation shows that our mean alignment effectively obtains domain-invariant node embeddings.

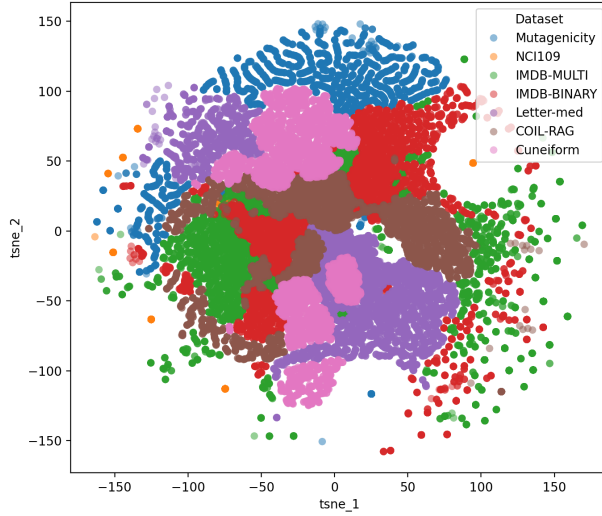


Figure 4: T-SNE visualization of aligned node embeddings of datasets from different domains.

H.10 Ablation Study

To verify the effectiveness of our proposed methods and modules, we conduct ablation study on global multi-graph construction, mean alignment algorithm, and reference layer. For the global multi-graph, we vary the number of multi-graphs from 1 to 6. Figure 5 and Figure 6 demonstrate the impact of the number of kernel parameters on downstream few-shot graph classification accuracy. These results were obtained by incrementally increasing the set of Gaussian kernel bandwidths from [0.25] to the full set [0.25, 0.5, 1, 2, 5, 10] used in our main experiments. It can be observed that classification accuracy improves with a greater number of global multi-graphs, particularly for datasets with original continuous node attributes. This observation further illustrates that the global multi-graphs constructed by using different kernel parameters help capture patterns from original features.

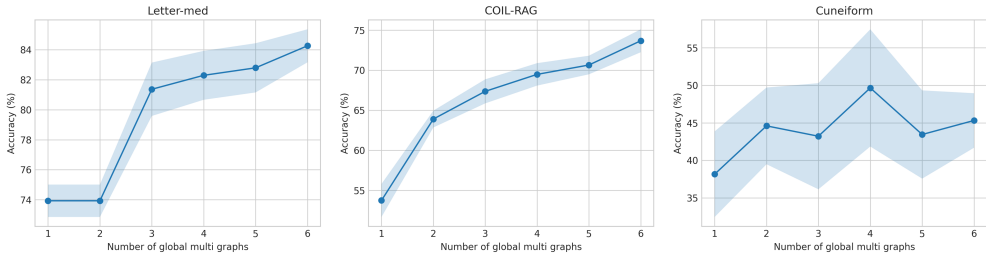


Figure 5: The few-shot graph classification accuracy in datasets with node attributes when the number of global multi-graphs increases from 1 to 6.

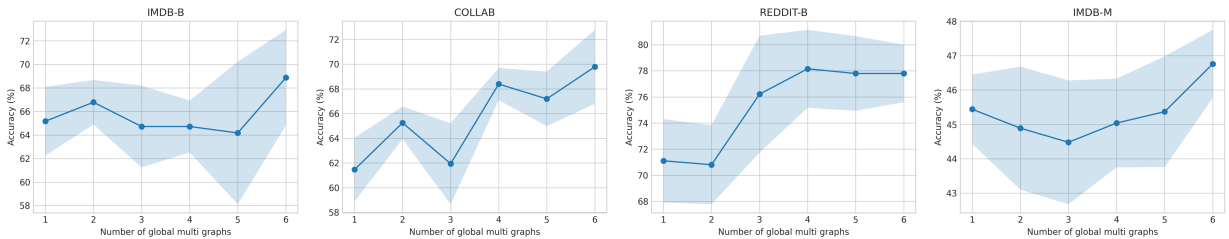


Figure 6: The few-shot graph classification accuracy in datasets without node attributes when the number of global multi-graphs increases from 1 to 6.

We conducted experiments using simple pooling without reference layers, and the results are presented in Table 14. After removing the reference layer module, the performance on all datasets shows degradation, especially on COLLAB, IMDB-BINARY, and Cuneiform. By removing the mean alignment, the performance on COLLAB, Letter-Med, and Cuneiform shows an evident decrease. Similarly, we also conduct experiments that remove the alignment module and both the alignment module and the reference layer. The overall impact of the two modules is shown in Table 15.

Table 14: Ablation study of reference layer and mean alignment module.

Model Variant	Dataset						
	COLLAB (50-shot)	REDDIT-B (50-shot)	IMDB-B (50-shot)	IMDB-M (50-shot)	Letter-med (50-shot)	COIL-RAG (5-shot)	Cuneiform (1-shot)
Original Model	68.09 \pm 2.99	81.52 \pm 1.50	68.39 \pm 4.06	46.70 \pm 0.99	85.60 \pm 1.44	74.20 \pm 0.77	55.86 \pm 8.15
Mean Readout Only	65.04 \pm 2.75	77.79 \pm 3.11	61.78 \pm 2.59	46.07 \pm 2.60	83.17 \pm 0.99	72.87 \pm 1.26	41.04 \pm 3.64
w/o alignment	64.90 \pm 1.81	76.74 \pm 5.43	66.06 \pm 4.44	45.78 \pm 1.46	81.87 \pm 1.31	72.14 \pm 0.35	42.87 \pm 5.18

Table 15: The individual effect of alignment algorithm and reference layer on downstream cross-domain graph classification. The reported performance is averaged on 7 datasets.

Alignment	Reference layer	Avg. Acc. (%)
✓	✓	68.62
✓	✗	63.95
✗	✓	64.37
✗	✗	63.16

H.11 Robustness Evaluation on Noisy Input Graphs

To validate our model’s performance on noisy graph data, we randomly added/deleted 10% edges to 50% of the test graphs during the few-shot test phase, and the results are shown in Table 16. It can be observed that there is only a slight decrease in terms of accuracy when the input graphs are perturbed or noisy, which demonstrates the robustness of our model.

Table 16: Few-shot graph classification performance comparison between original input and perturbed input

Dataset	REDDIT-B 50-shot	IMDB-B 50-shot	IMDB-M 50-shot	Letter-med 50-shot	COIL-RAG 5-shot	Cuneiform 1-shot
Original Graphs	81.52 \pm 1.50	68.39 \pm 4.06	46.70 \pm 0.99	85.60 \pm 1.44	74.20 \pm 0.77	55.86 \pm 8.15
50% Perturbed Graphs	77.68 \pm 2.30	65.22 \pm 1.07	46.07 \pm 1.55	83.47 \pm 3.22	72.13 \pm 1.93	44.14 \pm 3.82

H.12 Time and Memory Consumption

To evaluate the computational cost and runtime of model pre-training, we conducted experiments on two datasets of different scales: the larger deezer_ego_net dataset (9,629 graphs) and the smaller ENZYME dataset (600 graphs), each for 10 epochs. The wall-clock time and peak GPU/RAM memory usage are presented in the Table 17. We also compared the wall-clock time and memory cost of pre-training with ProNoG [Yu et al., 2025c] and BRIDGE [Yuan et al., 2025a] on the same dataset. It can be observed that our GraphVec-FM requires less training time, especially on relatively large datasets. GraphVec-FM demands more memory consumption, which is primarily due to the computation and storage of the global graph.

To ensure fair comparison, since ProNoG and BRIDGE process 4 graphs at once, we set our model’s batch size to 4. All experiments are conducted on 14 vCPU Intel(R) Xeon(R) Gold 6348 CPU with one Nvidia A800-80G GPU, CUDA 11.8.

Table 17: Performance and resource utilization comparison

Method	deezer_ego_net			ENZYMES		
	wall-clock time (s)	GPU Peak Memory (GB)	RAM Peak Memory (GB)	wall-clock time (s)	GPU Peak Memory (GB)	RAM Peak Memory (GB)
ProNoG	1194.61	0.12	1.1	69.54	0.05	0.96
BRIDGE	1600.28	0.31	1.27	116.99	0.18	1.17
Our Method	899.22	1.04	46.42	76.15	0.26	8.35